Metal-Organic Frameworks in Motion

Review Article

Author(s):
Terzopoulou, Anastasia; Nicholas, James; Chen, Xiang-Zhong; Nelson, Bradley; Pané, Salvador; Puigmarti-Luis, Josep

Publication date:
2020-10-28

Permanent link:
https://doi.org/10.3929/ethz-b-000447744

Originally published in:
Chemical Reviews 120(20), https://doi.org/10.1021/acs.chemrev.0c00535

Funding acknowledgement:
677020 - Microfluidic Crystal Factories (μ-CrysFact): a breakthrough approach for crystal engineering (EC)
771565C - Highly Integrated Nanoscale Robots for Targeted Delivery to the Central Nervous System (EC)
181988 - Functional 2D porous crystalline materials (2DMats) (SNF)
743217 - Soft Micro Robotics (EC)

Metal-Organic Frameworks in Motion

Anastasia Terzopoulou[1Φ], James D. Nicholas[2,3Φ], Xiang-Zhong Chen[1], Bradley J. Nelson[1], Salvador Pané[1] and Josep Puigmartí-Luis[2,3,4]**

1. Institute of Robotics and Intelligent Systems, ETH Zurich, Tannenstrasse 3, CH-8092 Zurich, Switzerland
2. Institute for Chemical and Bioengineering, ETH Zurich, Vladimir-Prelog-Weg 1, CH-8093 Zurich, Switzerland
3. Departament de Ciència dels Materials i Química Física, Institut de Química Teòrica i Computacional, 08028 Barcelona, Spain.
4. ICREA, Pg. Lluís Companys 23, 08010 Barcelona, Spain.

*Email: vidalp@ethz.ch

*Email: josep.puigmarti@ub.edu

ΦThese authors contributed equally to this review.

Abstract

During the last two decades, engineering motion with small-scale matter has received much attention in several areas of research, ranging from supramolecular chemistry and colloidal science to robotics and automation. The numerous discoveries and innovative concepts realised in motile micro- and nanostructures have converged in the field of small-scale swimmers. These manmade micro- and nanomachines can move in fluids by transforming different forms of energy to mechanical motion. Recently, metal-organic frameworks (MOFs), which are crystalline coordination polymers with high porosity, have been proposed as key building blocks in several small-scale swimmer designs. These materials possess the required features for motile micro- and nanodevices, such as high cargo-loading capacity, biodegradability, biocompatibility, and stimuli-responsiveness. In this review, we take a journey through the major breakthroughs and milestones realised in the area of MOF-based small-scale swimmers. First, a brief introduction to the field of small-scale swimmers is provided. Next, we review different strategies that have been reported for imparting motion to MOFs. Finally, we emphasise the incorporation of molecular machines into the MOF's architecture as the means to create highly integrated small-scale swimmers. The strategies and developments explored in this review pave the way towards the use of motile MOFs for a variety of applications in the fields of biomedicine, environmental remediation and on-the-fly chemistry.

Table of Contents

1. Introduction

Micro- and nanoscale swimmers herald a new era of biomedicine and on-the-fly chemistry applications.[1–6] These small-scale devices have the ability to move through a variety of fluids by interacting with chemicals existing in their swimming environment, or by means of external energy sources such as magnetic fields,[7] electric fields,[8] ultrasound,[9,10] light,[11,12] or combinations of these.[13,14] Owing to their motion capabilities, small-scale swimmers have been proposed as therapeutic mobile carriers,[15] biopsy agents,[16] on-the-fly chemical sensors,[17] pollutant micro- and nanocleaners,[18] and metal scavengers.[19] It is important to clarify the nomenclature used to refer to micro- and nanoswimmers. Micro- and nanoswimmers are named distinctively as a function of the level of control of their motion: (a) small-scale motors refer to any micro- and nanostructure that converts an input of energy into motion; (b) small-scale robots refer to micro- and nanomotors, where the speed and trajectory are externally controlled by one or more energy source. Note that the term micro- and nanorobot is increasingly recognised in publications, but it is misused on some occasions to designate devices that swim erratically, such as chemically propelled micro- and nanoswimmers. Any mobile machine categorised as robot must involve some level of control, whether the control unit is exogenous, or integrated within the platform. A small-scale device must incorporate components for controlling both its trajectory and speed to be considered a micro- or nanorobotic device. As such, swimmers driven purely by chemical reactions should not be categorised as robots.

In the last two decades, the field of small-scale swimmers has gained considerable attention as combined efforts from several disciplines are continuously being made to address the unresolved challenges and limitations related to these devices.[20–23] This is particularly noticeable in the area of biomedical small-scale swimmers. While major research efforts initially addressed

the various designs for the locomotion of these devices in fluids,[24] today's focus is on meeting all the requirements for their translation into clinical applications.[25–27] Current features being investigated are their biocompatibility,[28] therapeutic loading capacity and cargo delivery efficiency,[29] monitoring and tracking,[30,31] and biodegradation and clearance.[32] New paradigms in materials and fabrication schemes are crucial to integrate all these features into a single device. It is indisputable that the first wave of micro- and nanoswimmers capitalised on advances made in micro- and nanomanufacturing technologies.[33] Despite new advances in technology, it is obvious that the next generation of micro- and nanoswimmers will undoubtedly benefit from concerted contributions from the disciplines of materials science and chemistry, in specific areas that were previously disconnected to the field of micro- and nanoswimmers.[34] A recent example of this new wave is the incorporation of soft materials such as polymers,[35–37] gels,[38,39] or macromolecules.[40,41] These materials not only facilitate the creation of small-scale swimmers with more complex locomotion mechanisms, they also allow for advanced capabilities such as morphological adaptability,[42] optimal compliance with tissues,[43] and enhanced biocompatibility,[44] and biodegradability.[45]

From the considerable diversity of soft materials, metal-organic frameworks (MOFs) have emerged as prospective materials for a manifold integration of multiple functions into a single device. MOFs are a class of crystalline porous coordination polymers constructed from metal ions (or clusters) interconnected by means of organic ligands. Their highly ordered porous structure and high surface area provide MOFs with a high loading capacity for therapeutic cargoes such as drugs or active biomolecules.[46] Additionally, the vast available library of ligands and metal ions enables the fine-tuning of their porosity[47,48] (a feature that facilitates control over their loading capacity and the interaction/delivery of cargo),[49] in addition to harnessing their functions (e.g.

MOFs incorporating magnetic components have also been used successfully in magnetic resonance imaging (MRI)).[50,51] Furthermore, several MOFs have exhibited biocompatibility characteristics and biodegradability.[52,53] Accordingly, MOFs possess many of the features required to achieve a new generation of highly integrated micro- and nanoswimmers for biomedical applications. Despite this, the integration of MOFs in small-scale swimmers is not widely reported in the literature, although new advancements in this domain are highly envisioned in the near future.[54] MOFs in motion have the potential to change the future landscape of small-scale swimmers and their areas of application, for example, by enabling the successful translation of micro- and nanoswimmers into clinical practice.

In this review, we aim to provide an up-to-date overview of the recent progress made in the fabrication of MOF-based micro- and nanoswimmers. Additionally, we will also cover a section on the integration of molecular switches onto MOF architectures. Molecular switches perform well in solution where reversible and controllable transformations between two or more states can be accomplished upon exposure to external stimuli (likewise in micro- and nanoswimmers). However, in solid state, molecular switches can experience difficulties in their operation due to restrictions imposed by their movement. Recent work has shown that the immobilisation of molecular switches onto highly ordered porous structures such as MOFs not only favours their free motion in the pore, it also enables their precise arrangement in space, thus preventing their agglomeration, malfunctioning, and subsequent failure. This research represents a new and exciting field where a marriage between artificial supramolecular machinery and MOFs is expected to open new avenues in the design of artificial living matter.[55–57] We will conclude this review with our perspective on the remaining challenges and opportunities that lay ahead in the emerging and fast-growing field of micro- and nanoswimmers.

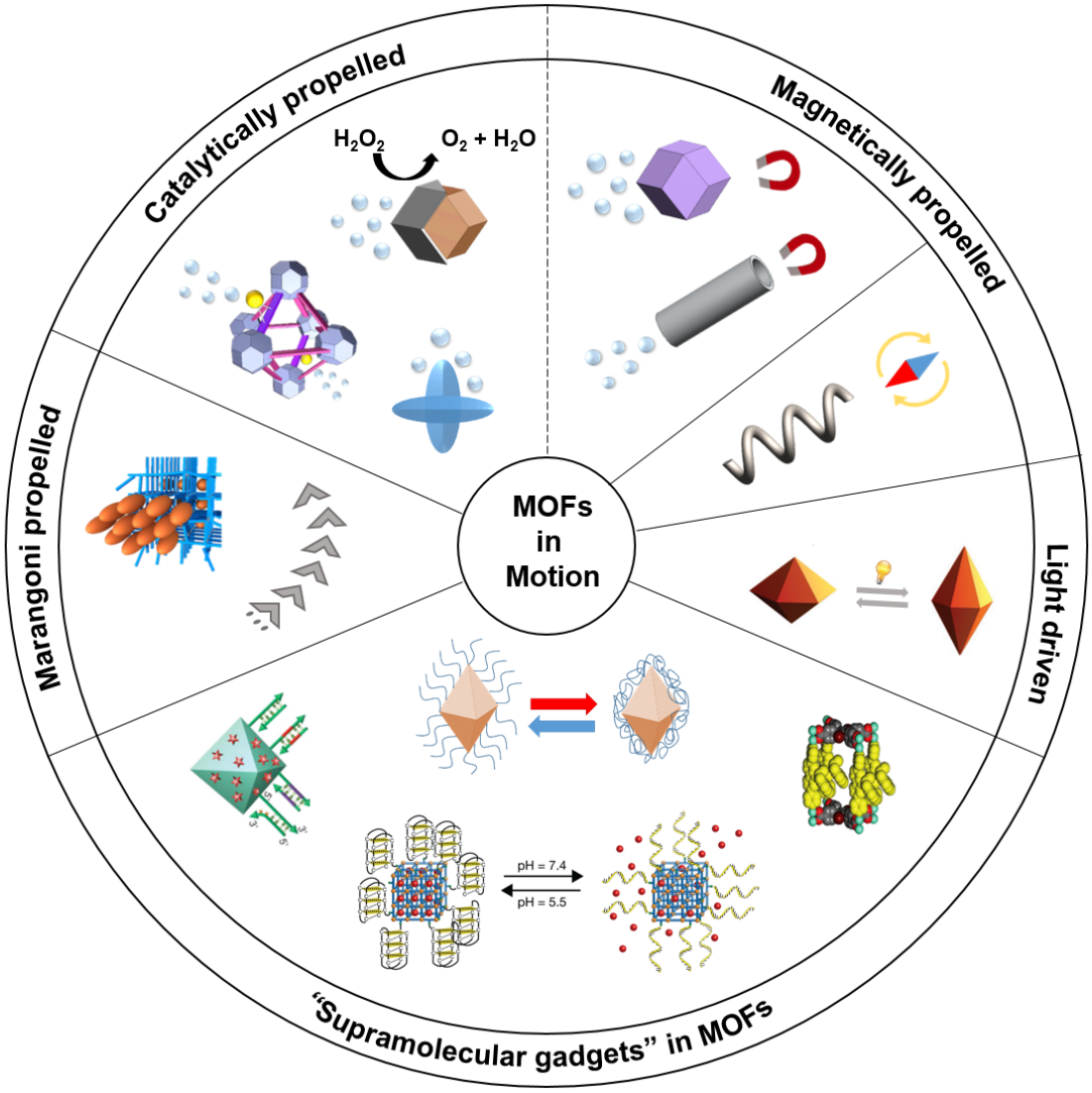

Figure 1. Recent advances in MOFs in motion. MOF crystals propelled via surface tension gradients, catalytic reactions, magnetic fields and light. MOFs functionalised with supramolecular gadgets which are responsive to external stimuli. Figure 1. Reproduced with permission from Refs 58, 59. Copyright Springer Nature 2012, 2019; Refs 60–62. Copyright John Wiley and Sons 2019, 2018, 2016; Ref 63. Copyright American Chemical Society 2017; and Ref 64. Copyright Royal Society of Chemistry 2015.

2. Fuel bearing MOF-based swimmers

Arguably, research in small-scale swimmers traces its roots back to the late 1970s with Purcell's instructive analysis on the motion strategies of microorganisms in low Reynolds number media where viscous forces dominate. In his famous talk "Life at low Reynolds number", Purcell provided the clues for the engineering of a wide range of micro- and nanoscale swimmers.[65] Summarising Purcell's interpretations, the key for achieving motion at small scales consists of breaking the time reversal symmetry of the flow (i.e. the Scallop theorem). This condition can, for example, be accomplished with the incorporation of machinery that allows for a non-reciprocating motion mechanism (e.g. waving an elastic appendage or rotating a chiral arm). Alternatively, the integration of a component that generates (or experiences) a force in response to a field or gradient is also a means to achieve motion at the micro- and nanoscale (*vide infra*).

In this context, nature provides countless examples of non-reciprocating motion mechanisms or motion due to a gradient in the concentration of chemical species.[26] Flagellated bacteria, for example, can swim by rotating a chiral arm (i.e. a helical flagella).[66] We also know that bacteria can move freely in solution towards specific locations by following the direction where the concentration of nutrients increases. This mechanism, known as chemotaxis, is key to establishing the dynamics, communication, and the collective behaviour of microorganisms.[67] Additionally, concentration gradients can also lead to gradients in surface tension at the interface of two immiscible phases, which result in Marangoni flows.[68] Marangoni flows can concomitantly generate a net force that can pull one of the two phases (e.g. a liquid or a solid) away from the regions of lower surface tension (i.e. the "Marangoni effect"). Certainly, in the field of micro- and nanoswimmers, researchers have drawn inspiration from these processes to design, for example, MOF-based Marangoni propelled swimmers.[69]

2.1. Marangoni propelled MOF-based swimmers

The first MOF-based swimmer ever reported dates back to 2012 when Matsui, Kitagawa and co-workers designed MOF crystals (i.e. $[Cu_2L_2ted]_n$, where L is 1,4-benzenedicarboxylate and ted stands for triethylenediamine) that incorporated self-assembling peptides in their pores, i.e. diphenylalanine (DPA).[58] The authors demonstrated that the release of DPA upon the addition of ethylenediaminetetraacetic acid (EDTA) led to the generation of a surface tension difference at the water/MOF interface, which resulted in the motion of the MOF via the Marangoni effect (Figure 2a). As expected, the MOF crystals moved towards areas with higher surface tension. Interestingly, it was demonstrated in this study that the main trigger in the locomotion was the self-assembly process exerted by the peptide molecules upon their release from the MOF network when in contact with water. The authors observed that when other hydrophobic molecules such as phenol and phenylalanine were incorporated into the MOF network instead of DPA, the MOF crystals lost their motion capabilities. This halt in the motion of the MOF crystals proved to be related to the poor self-assembly capacity of these hydrophobic molecules in the reaction media. Furthermore, this pioneering study also showed that the porous crystalline network is key to enable the generation of Marangoni flows, and hence, for the locomotion capabilities of the MOF crystals. The authors demonstrated that when DPA was added to an aqueous solution containing EDTA, the DPA molecules alone could not self-organise at the air/water interface. Accordingly, this controlled experiment demonstrated that a pre-organisation of the DPA molecules in the porous crystalline network was essential for the MOF crystals to swim, which clearly illustrates the impact and added value of MOF features in the field of micro- and nanoswimmers. However, this study did not demonstrate the speed and trajectory of the MOF-based Marangoni propelled swimmers.

In a follow up study, the same group also confirmed that a directional motion of the above mentioned DPA loaded MOF could be programmed with the generation of a pH gradient in solution.[70] In this work the authors took advantage of the reduced capacity of DPA molecules to self-assemble in basic environments to stop their motion (Figure 2b). In addition to EDTA, which enabled the generation of Marangoni flows at the water/MOF interface through the dissolution of the MOF network, PbSe quantum dots (QDs) functionalised with enzyme urease and an acidic post were also immersed in the aqueous solution. While urease could locally increase the pH near the PbSe QDs via the generation of NH_3, the acidic post ensured the occurrence of a pH gradient in the aqueous media. The authors observed that the MOF crystals could autonomously move in solution while sensing the established pH gradient. Indeed, the MOF crystals stopped moving near the PbSe QDs where the pH was higher. As indicated above, the higher the pH the lower the ability for DPA molecules to self-organise at the water/MOF interface, leading to a loss of the Marangoni flows, and hence, to the eventual cease of the MOF locomotion capabilities. While the autonomous locomotion of these MOF crystals is clearly mimicking the chemotaxis of microorganisms, these fuel-bearing MOF-based swimmers cannot control their motion in an on-demand on/off fashion, and further, they readily dissolve in the EDTA solution over time, which irreversibly stops the locomotion.

To demonstrate speed control and directionality on the motion of Marangoni propelled MOF-based swimmers, Grzybowski and co-workers explored the effect different features have on the locomotion of this class of swimmers, including the shape of the MOF particles and the effect of the chemical nature of the fuel incorporated into their network.[71] For this study the authors used freestanding films of a porphyrin-based MOF, i.e. PCN-222 (or $Zr_6O_8L_3$, where L stands for meso-tetra(4-carboxyphenyl)-porphyrin), which could incorporate different solvents in its structure (e.g.

benzoic acid (BA), dimethylformamide (DMF), diethylformamide (DEF), or dibutylformamide (DBF)). These solvents when released from the MOF network could potentially behave like DPA and generate surface tension gradients at the water/PCN-222 film interface, thus enabling the locomotion of the films. PCN-222 films with circular disk shapes and symmetric and asymmetric compact polygons (e.g., squares or rectangular bars) were fabricated by simply cutting the robust PCN-222 films into the desired form (Figure 2c). While circular shapes moved randomly in solution due to the release of the solvent incorporated in the MOF network, polygons with symmetric shapes tended to display circular orbits (Figure 2d), whereas asymmetric V-shaped films moved in a spiral trajectory with the spike-end leading (Figure 2e). Accordingly, this work demonstrates that shape plays a key role in the directionality of the swimming object. Interestingly, the authors observed that the speed of the MOF films increased by increasing the length of the alkyl chain of the solvent entrapped in the MOF matrix. That is, MOF films incorporating DBF displayed higher speeds, approximately 210 $mm \cdot s^{-1}$, while for BA powered films the speed of the MOF particles was ca. 120 $mm \cdot s^{-1}$. Surprisingly, the authors showed that these Marangoni propelled MOF-based swimmers could be refuelled by simply adding new DBF onto the MOF film. Therefore, in sharp contrast to the previous studies highlighted above, the motion of the fuel bearing MOF-based swimmers was not defined by the initial amount of fuel loaded in the MOF matrix. However, these swimmers could not maintain the same rate of motion for a prolonged period, nor did they achieve 3D motion capabilities. To overcome these limitations of fuel bearing MOF-based swimmers, researchers developed new MOF-based motors that could harvest energy from their surrounding environment.

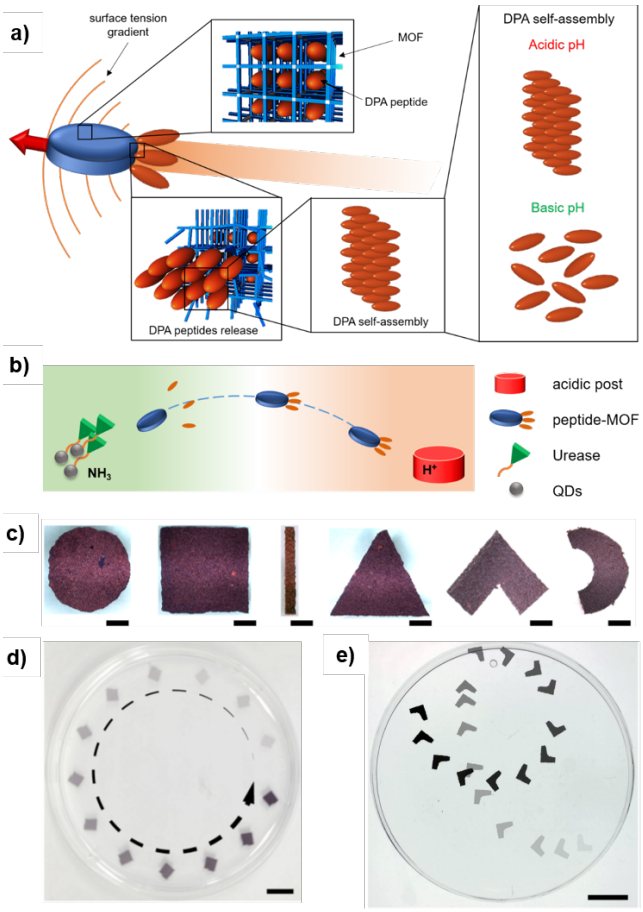

Figure 2. Asymmetric surface tension driven MOF-based machines. a) Schematic of the mechanism of DPA-MOF motion. DPA peptides are incorporated in the nanoscale pores of the MOF. The released and reassembled DPA peptides form the hydrophobic domain at the end of MOF particle, lowering the surface tension on that side. The MOF particle moves towards higher surface tension via Marangoni effect. b) Scheme of directed motion of peptide-MOF motors towards higher pH. PbSe quantum dots (QDs) functionalised with enzyme urease generate NH_3, locally increasing the pH of the solution in the target area. The peptide-MOF motor starts swimming towards higher pH. The movement is completed at the target due to basic pH. c) PCN-22 films cut in various shapes. d) A square film performs circular orbit, while e) V-shaped particles are moving with the spike end pointing forward. Portions of figure reprinted with permission from Springer, Nature Materials, reference [58] Copyright 2012, references[70,71] Copyright 2015, 2017 American Chemical Society.

3. Catalytically propelled MOF-based swimmers

Catalytically propelled small-scale swimmers are a subclass of chemically driven motors that incorporate a catalytic component within their chassis.[72] The catalyst interacts with reagents present in the swimming environment by increasing the rate of a specific reaction, the products of which ultimately induce the propulsion of the device. Therefore, catalytically propelled small-scale swimmers differ from Marangoni propelled ones in that they do not deliver fuel to the swimming environment, but rather consume from it.

Three main mechanisms have been identified for the locomotion of catalytically propelled small-scale swimmers: (a) bubble propulsion; (b) diffusiophoresis and (c) electrophoresis.[73] Bubble propulsion refers to the motion mechanism in which gas bubbles generated by the catalysed reaction impart momentum to the motor when bubbles asymmetrically detach from the motor's catalytic surface.[74] Motion by self-diffusiophoresis is caused when a product concentration gradient is created around the swimmer as a consequence of the catalytic reaction occurring at one region of the swimmer. Self-electrophoresis is a propulsion mechanism exhibited by swimmers consisting of two interconnected metals that act respectively as the cathode and the anode of an electrochemical battery.[75] As a result of the electrochemical reactions taking place at each metal, a concentration gradient of ionic species is produced, which in turn generates an electric field that causes the motion of the swimmer. One of the most broadly investigated fuels in the field of catalytic motors is hydrogen peroxide, as its decomposition can occur both chemically and electrochemically. This reaction can be catalysed by several metals, alloys and metal oxides, platinum being the most utilised catalyst in this type of motor. Several Pt-based motor architectures with the above-mentioned mechanisms, using hydrogen peroxide as a fuel have been reported so far.[76]

Catalytic propulsion of MOF crystals was first demonstrated by Chin and co-workers.[77] The researchers synthesised MOF-based Janus micromotors consisting of zinc 2-methylimidazolate (ZIF-8) crystals half-coated with a catalytically active cobalt(II) 2-methylimidazolate (ZIF-67) film. To fabricate the Janus architecture, ZIF-8 crystals were partially embedded in a polymeric film so that the exposed ZIF-8 surface could be half covered by an epitaxially grown layer of ZIF-67. The Janus microstructures were released upon selective dissolution of the polymer film. The swimmers exhibited bubble propulsion when placed in a solution containing hydrogen peroxide. Ejection of bubbles took place from the ZIF-67 face of the Janus particle, where cobalt(II) nodes act as catalyst. Asymmetrisation of MOF micro- and submicrocrystals with metallic layers to form Janus motors was later reported by Maspoch and co-workers.[78] The swimmers were created by forming a monolayer of MOFs by drop casting their solution onto a substrate. Subsequently one or more layers of different metals (Au, Co, Pt) were sputtered (Figure 3a). Both ZIF-8 and UiO-66 (Universitet i Oslo, zirconium(IV) terephthalate) with various particle sizes were partially coated using this approach (Figure 3b). The researchers showed the potential of multilayer deposition of more than one metal, with Co and Au (Figure 3c). Bubble propulsion was demonstrated when Janus motors containing a single Pt layer (Figure 3d-e) were immersed in solutions containing H_2O_2 and sodium cholate, the latter a surfactant used to control the size of the bubbles. While the authors demonstrated the integration of ferromagnetic cobalt layers and the responsiveness of the swimmers to magnetic fields, no magnetic control was demonstrated. Bubble propulsion of catalytic MOF-based Janus micromotors was also achieved later by Ding and co-workers with asymmetric deposition of Ag on ZIF-Zn-Fe polymer composite microspheres.[79] The swimmers were fabricated by embedding ZIF-Zn-Fe in polystyrene beads. A hemispherical silver layer was integrated by sputtering a monolayer of beads dispersed on a glass

substrate. In this example, Ag served as the catalytic component for the decomposition of H_2O_2, which enabled the motion of the Janus system by bubble propulsion. Interestingly, the introduction of iron(II) into the network of ZIF-8 allowed these motors to be used as water-pollutant motile microcleaners. When immersed in a solution containing both H_2O_2, the iron(II) nodes of the ZIF-Zn-Fe reacted with H_2O_2 to generate reactive oxygen species, which in turn could degrade organic pollutants such as rhodamine B. This initial research on chemically propelled MOFs was primarily focused on achieving catalytic motion, and control over their motion was not really demonstrated.

In 2017, Wang, Cohen and co-workers reported for the first time UiO-67, (zirconium(IV) 4, 4'-biphenyldicarboxylate)-based swimmers with chemical control capabilities over their speed. The UiO-67 network integrated bipyridine ligands allowed for the metalation of the MOF with catalytically active metal centres (Co and Mn) (Figure 3f).[63] Decomposition of H_2O_2 on these metal sites enabled the bubble propulsion of the MOFs, the speed of which was dependent on the chosen metal centre (Figure 3g). Control over the propulsion of the MOF-based engines was achieved through a chemically induced braking mechanism that consisted of adding chelating agents such as iminodiacetic acid (IDA) or ethylenediaminetetraacetic acid (EDTA) into the swimming environment. These chelating species have an increased affinity to coordinate the catalytically active metal centres complexed by the embedded bipyridine. Upon chelation, the catalytic activity of the engine is suppressed, and therefore so is their propulsion (Figure 3h). While this research pioneered a chemical control over the propulsion of a chemically driven MOF, directionality of the motion was not addressed. The addition of the chemical brakes in the swimming environment would irreversibly stop the motion of the swimmers without the possibility of an on-demand on/off motion.

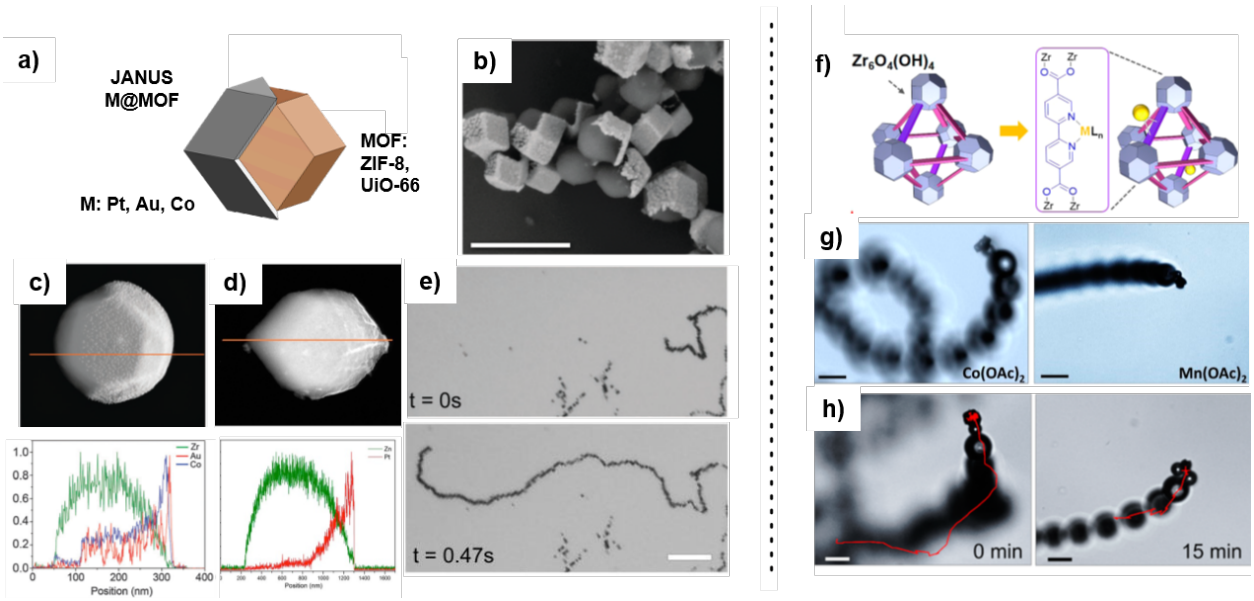

Figure 3. MOF composites presenting catalytic propulsion. a) Schematics of Janus metal@MOF (M@MOF) and b) SEM image of Au@ZIF-8 particles showing the asymmetric coating of the MOFs. c)-d) SEM images and elemental line scans showing distributions of metal content on single particles, including Au@Co@UiO-66 and Pt@ZIF-8. e) Optical microscopy images of motorised Pt coated Janus MOFs performing catalytic propulsion. f) UiO-type MOF based microengines highlighting the metallisation of the organic ligand. g) Tuning the propulsion speed of the MOF based engines based on different metals, here Co and Mn. h) Illustration of the braking mechanism, when adding chelators. The red trajectories correspond to the locomotion of the engine within two seconds at the moment the chelator is added and 15 min after interacting with the engine. e) is reprinted with permission from ref[78] Copyright 2016 Royal Society of Chemistry and h) is reprinted from ref[63] Copyright 2017 American Chemical Society.

An alternative approach using an enzyme instead of catalytically active metal centre to decompose H_2O_2 to O_2 to provide bubble propulsion to a MOF-based system was reported in 2019 by Ma *et al.*[80] This work utilised a dual enzyme-functionalised ZIF-8 loaded with upconversion nanoparticles and photosensitiser to enhance synergetic photodynamic therapy (PDT) and starvation therapy (ST) for cancer treatment. This work is interesting as it uses two enzymatic

cascade reactions to provide both the therapeutic effect and propulsion of the nanomotor. First, glucose acts as the primary fuel, which is decomposed by glucose oxidase (GOx) to produce H_2O_2. This is followed by subsequent decomposition of the H_2O_2 intermediate with catalase (CAT)[81] to produce H_2O and O_2. Here the O_2 produced not only propels the MOF nanomotor, but also allows subsequent generation of singlet oxygen required for PDT. Whilst a small degree of control over the motion is achieved due to the dependence on the glucose concentration for catalysis by GOx, the resulting motion is random and not directionally controlled, similarly to the previous examples described. This has the positive effect of enhancing diffusivity of the nanomotor, and hence improved cellular uptake was observed in studies with human epithelial cervix adenocarcinoma (HeLa) cells, but no specific targeting control is obtained.

The lack of control over the trajectory and speed of MOF crystals purely driven by catalysis restricts their potential for use in specific applications, especially in the biomedical area, where on-demand adjustment of the motor kinematics is crucial to accomplish specific tasks such as reaching a specific tissues or precisely manipulating small objects. For chemically propelled MOFs to qualify as small-scale robots (MOFBOTs), additional components allowing for both their steerability and speed control are necessary.

3.1. Catalytic propulsion with pH control

Developments towards the goal of a controllable catalytically propelled MOF-based device were described by Chen, Liang and co-workers who reported a pH-responsive ZIF-L (a 2D layered version of ZIF-8) micromotor.[82] In this work, the MOF was functionalised with CAT to decompose H_2O_2 to O_2 to provide bubble propulsion, and succinylated β-lactoglobulin was incorporated to act as a pH-responsive gatekeeper, preventing or allowing the fuel to reach the catalase. At pH > 5,

the β-lactoglobulin was permeable to the H_2O_2 fuel, and so could access the catalase and allow the micromotor to be propelled. However, at pH < 5, β-lactoglobulin undergoes a conformational change and becomes impermeable to the fuel. This prevents the production of the bubbles and effectively switches the motor off, providing an alternative mechanism for speed control in addition to varying the concentration of H_2O_2 fuel. However, the motion of the micromotor was still not controlled directionally, and though integrating an effective on-off switch is a useful element of control, to provide full robotic functionality in a real-life application, it would likely require additional stimuli-responsive elements to provide more directional control.

Building on this work, Chen, Liang and co-workers then reported a MOF micromotor for which changes in pH could be used to control vertical motion of the particles through buoyancy effects, so that the micromotor could be made to rise or sink based on the pH environment.[83] In this system, ZIF-L was again functionalised with CAT to provide O_2 gas bubble generation, but this time the polymer poly(2-diisopropylamino)ethyl methacrylate (PDPA)[84] was used to provide the pH responsive element. At pH > 6.4, the tertiary amine groups of PDPA are deprotonated, leading to hydrophobicity of the polymer and subsequent adsorption of the catalytically generated O_2 bubbles to the polymer. This reportedly led to an increase in the buoyancy of the microparticles, leading to an ascending motion. In contrast, at pH < 6.4, the amine groups are protonated and the polymer is hydrophilic, meaning that O_2 molecules were desorbed and the particles descended (Figure 4a). Due to the size of the microparticles, motion was only observed when the polymer was deprotonated, as the propulsion alone was not enough to drive the device, and instead movement was reliant on the buoyancy effect. A demonstration of how the device could be potentially used for selective drug delivery was achieved by loading the micromotors with the anticancer drug, fluorouracil (5-FU). MCF-7 breast cancer cells were grown on the top and bottom

wall of a chamber, and using buffers at different pH, motion was controlled to deliver the drug-loaded micromotors. Upon internalisation and degradation of the MOF-micromotors, the drug would be released into the cells and kill them. At pH 6.3, only the cells at the bottom of the chamber were significantly affected, with cell viability < 2 %, whilst those at the top retained over 95 % viability. Conversely, at pH 7.4 the cells at the top of the chamber demonstrated a reduction to less than 39 % viability, compared to over 82 % viability of the cells at the bottom, indicating that the majority of the micromotors could be effectively directed to the target cells by controlling the pH (Figure 4b). Control experiments with non-drug loaded micromotors also showed no reduction in cell viability of either top or bottom cells at either pH, indicating the micromotors themselves did not affect cell viability. The ability for the micromotors to be switched between different pH environments and retain the ability to rise and descend over multiple cycles was also investigated, as this would be an important property for the devices if deployed in a biomedical application. The directional control was shown to be preserved after at least 4 sweeps, with the particles moving to the top when in pH 7.4 buffer solution, and then sinking when HCl solution with H_2O_2 was added, and subsequently rising again when most of the solution was removed and replaced with the pH 7.4 buffer again.

However, arguably, the current practicality of the method is somewhat limited by the single direction of motion control available, and so further work is necessary to extend the applicability and prove that the buoyancy could be controlled with a pH gradient rather than just in bulk buffer solutions, which would be advantageous in a biomedical application. If these were achieved, it would demonstrate a useful application of MOF-based swimmers in the field of drug delivery devices.

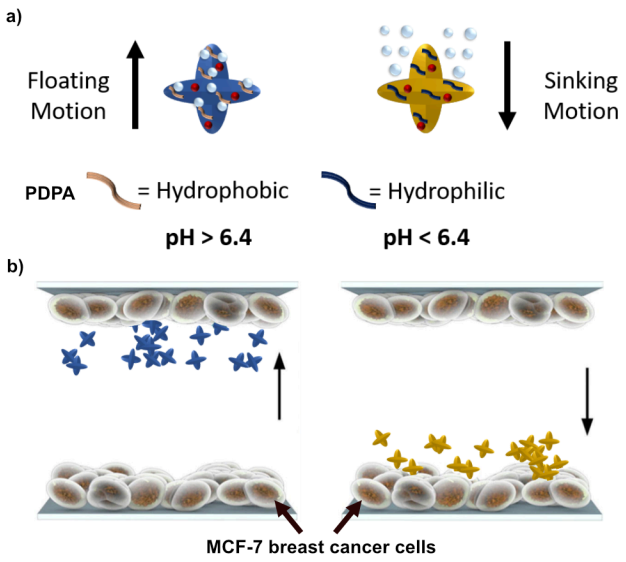

Figure 4. Catalytically propelled, pH controlled ZIF-L based micromotor - CAT-PDPA@ZIF-L. a) Schematic illustration showing the behaviour of the micromotor at pH above and below 6.4. At pH > 6.4, deprotonation of the tertiary amine groups of PDPA make it hydrophobic. CAT (represented in red in the figure) catalyses the production of O_2 bubbles from H_2O_2, which bind to the PDPA, increasing the buoyancy of the device and leading to an ascending motion. At pH < 6.4, PDPA is hydrophilic as the amine groups are protonated, which leads to gas bubble dissociation from the micromotors, triggering particle-descending motion. b) Schematic illustration of the micromotor motion in a cell culture chamber, where at pH 7.4 drug-loaded micromotors ascend and deliver the drug to cells located at the top of the chamber, while at pH 6.3 the micromotors sink and the drugs are delivered to cells at the bottom of the chamber. Reprinted from reference[83] Copyright 2019 with permission from Elsevier.

3.2. Catalytic propulsion with magnetic control

The integration of magnetic building blocks in catalytic MOF-based motors can add a certain level of control to these swimmers, especially in terms of their steerability.[85] This approach was adopted by Wang *et al.*, who reported the use of a ZIF-based micromotor consisting of ZIF-67 microcrystals, the surface of which was decorated with Fe_3O_4 nanoparticles (Figure 5a-b).[86] The

cobalt(II) nodes of ZIF-67 served as the units for the catalytic propulsion, while magnetite nanoparticles rendered the swimmers magnetically steerable (Figure 5c). The swimmers were also loaded with the anti-cancer drug doxorubicin. Interestingly, the catalytic decomposition of H_2O_2 at the cobalt centres and the hydrolysis of ZIF-67 due to the affinity of water to cobalt(II) led to changes in the pores and structure of the MOF, which enabled the release of doxorubicin. While the fuel enabled both the motion of the swimmer and the release of its therapeutic cargo, this effect significantly limits its applications, as the drug will be constantly leaked during the journey of the micromotor to the target destination (Figure 5d), thus decreasing its delivery efficacy.

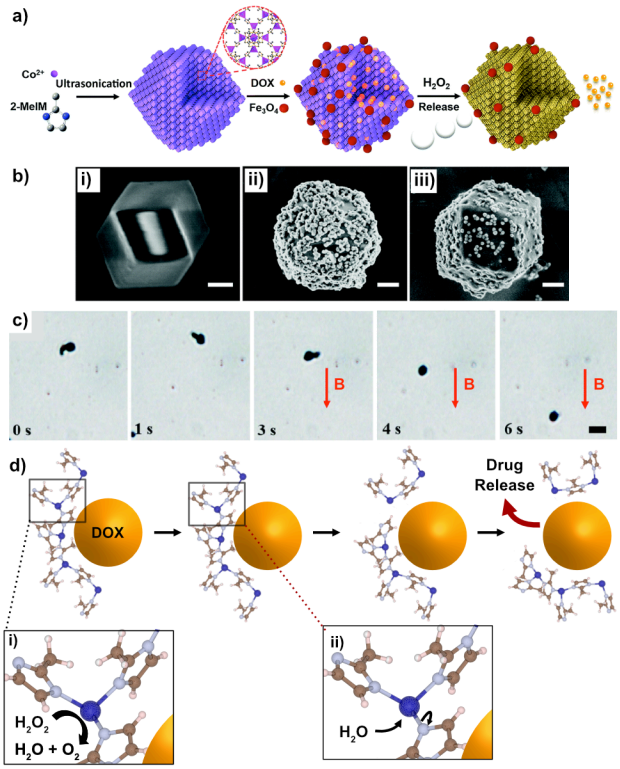

Figure 5. Catalytically propelled, magnetically controlled ZIF-67 based micromotor. a) Schematic illustration of fabrication of ZIF-67/Fe_3O_4/DOX micromotor and drug delivery mechanism. The micromotor is synthesised by ultrasonication, then loaded with DOX and Fe_3O_4. Addition of H_2O_2 fuel

causes release of DOX through a change in the structure of the ZIF, indicated by the change in colour from purple to yellow. b) SEM images of i) ZIF-67, ii) ZIF-67/Fe_3O_4, and iii) ZIF-67/Fe_3O_4/DOX micromotors, showing that the rhombic dodecahedral shape is maintained after functionalisation. Scale bar: 1 μm. c) Time-lapse images showing the motion of the micromotors under applied magnetic field, B, (direction depicted by arrow) in a 4 % H_2O_2 solution containing 0.33% Triton X-100. Scale bar: 10 μm. d) Schematic illustration of catalytic decomposition of H_2O_2 at the Co atoms in the ZIF structure (i) followed by hydrolysis of H_2O at the Co atoms (ii), leading to degradation of the structure and release of the drug. a-c) Reprinted with permission from reference[86] Copyright 2018 Royal Society of Chemistry.

Magnetic control of ZIF-8-based catalytic small-scale motors has also been recently demonstrated. In this case, due to the catalytic inactivity of ZIF-8 for decomposing H_2O_2, it was necessary to incorporate additional catalytic building blocks. Li *et al*. synthesised ZIF-8-based catalytically propelled microjets using kapok fibres as a template (Figure 6a).[87] The main body of the tubes were made of a magnetic mixed metal oxide comprising γ-Fe_2O_3 and γ-Al_2O_3. The outer and the inner cavities of the tubes were decorated by catalytic MnO_2 nanoparticles. Finally, ZIF-8 was grown on the outer surface of the tubes. In this configuration, the catalytically active MnO_2 was only accessible by the fuel at the inner surface, which allowed the microjet to swim by bubble propulsion. Magnetic steering was demonstrated by applying an external magnetic field, which could be used to direct the motion of the microjets as desired (Figure 6b, c). The ZIF-8 coating here was employed as an absorbent of the organic pollutants Congo red and doxycycline. The enhanced micromixing caused by the motion of the microjets boosted the adsorption capacity of ZIF-8. The reusability and chemical stability of the microswimmers were also demonstrated.

Pumera and co-workers also developed magnetically guided ZIF-8-based catalytic micromotors using a template-based interfacial synthesis (Figure 6d).[88] The approach was highly

versatile as it allowed swimmers of different dimensions to be produced. Briefly, the process began by infiltrating Fe_3O_4 nanoparticles through the smooth side of a porous polycarbonate membrane. The membrane was then carefully placed on the surface of an aqueous solution of the metal salt precursors ($Zn(NO_3)$, $FeCl_2$) for the synthesis of iron-doped ZIF-8. After a given time, a 1-octanol solution containing the ligand 2-methylimidazole was carefully added on top of the membrane, leading to Fe_3O_4–Fe-ZIF-8 rod-like microstructures. Next, deposition of catalytic platinum nanoparticles membranes was realised on one end of the rods still embedded in the membrane. Finally, by selectively dissolving the membrane, the Fe_3O_4–Fe-ZIF-8-Pt microswimmers were released. Here, Fe_3O_4 was used for magnetic guidance, while Pt enabled the catalytic bubble propulsion (Figure 6e). ZIF-8 was doped with iron(II) to provide chemical stability to the MOF component, as ZIF-8 is susceptible to degradation in H_2O_2 and acidic solutions. The microswimmers were also manipulated using a permanent magnet and in the absence of H_2O_2 fuel. The swimmers exhibited both rotational and translational motions, and they were able to follow a pre-planned path (Figure 6f). The swimmers were also successfully tested for environmental applications. The Fe-ZIF-8 served as an adsorbent to trap uranium (UO_2^{2+}) from radioactive wastewater. In-depth analysis showed that Fe(II) also played a crucial role in enhancing the removal of uranium, as it contributed to partially reduce U(VI) to U(IV).

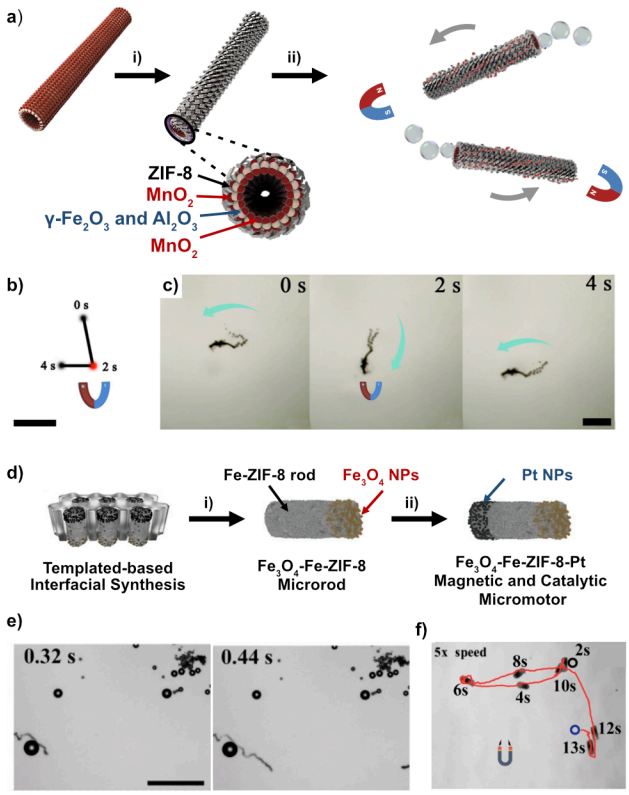

Figure 6. Catalytically propelled, magnetically controlled, ZIF-8-based micromotors. a) Schematic illustration of template-assisted synthesis, subsequent propulsion using H_2O_2 catalytic decomposition, and directional control using external magnetic fields of ZIF-8-γ-Fe_2O_3/γ-Al_2O_3/MnO_2 (ZIF-8-M). b) Illustrated trajectory of ZIF-8-M under magnetic field control, and c) corresponding time-lapse images. Scale bar: 200 μm. d) Schematic illustration of template-assisted synthesis of Fe_3O_4-Fe-ZIF-8-Pt. e) Time-lapse of magnetically controlled motion in 5 wt. % H_2O_2. Scale bar: 250 μm. f) Schematic illustration of the magnetically controlled, H_2O_2 catalysed propulsion, removal of uranium from solution, with proposed mechanism. g) Magnetically controlled translation behaviour of the micromotor (no H_2O_2 propulsion). a) and b) are adapted from reference[87] Copyright 2019 with permission from Elsevier. d) and e) are adapted from ref[88] Copyright 2019 American Chemical Society.

Catalytically propelled MOF-based swimmers with magnetic control directionality have shown promise in the field of environmental applications. However, in all the catalytically propelled MOF based machines presented so far, the implementation of H_2O_2 as fuel to drive the propulsion restricts their applicability to very specific chemical conditions. More biocompatible materials and application-specific relevant fuels need to be investigated for their translation into clinical practice. Non-MOF-based micromotors using alternative fuels such as urea and adenosine 5'-triphosphate (ATP) for propulsion in physiological conditions can be used as inspiration for the development of similarly fuelled MOF-based micromotors.[89,90] Indeed the propulsion mechanism of the MOF nanomotors used for cancer therapies in the work of Ma *et al*. discussed above was previously reported in 2008 by Feringa *et al*., in which carbon nanotubes were propelled by O_2 bubbles produced from the same glucose/GOx and H_2O_2/CAT enzymatic reactions.[91] Further advances in the field have shown that catalytic propulsion can also be achieved in water, as well as in gastrointestinal fluid.[92] These examples clearly illustrate both the advantages and current shortcomings of catalytically propelled machines. Replacing the metal sites and the inorganic particles that promote the fuel reactions with enzymes and biodegradable materials are the first steps towards developing catalytically propelled MOF-based swimmers for biomedical applications.

4. Light driven MOF-based actuators

Light as an external stimulus is a versatile means to control or power micro- and nanomachines.[11] Light can be applied remotely and can be controlled spatially and temporally in an effective and efficient manner.[93] In certain cases, light can induce secondary effects, such as photothermal phenomena, a property that can also be exploited for the activation of micro- and nanoswimmers.[94] Polymers and elastomers are among the most widely explored photoresponsive materials.[95]

Combining such soft materials with functional features intrinsic to MOF crystals could drive a new era in the field of advanced integrated small-scale robotics that can be controlled with external stimulation.

An ingenious way of exploiting the swelling behaviour of MOFs for the fabrication of micro- and nanoswimmers was presented by Maspoch and co-workers.[60,96] The authors implemented a pre-programmed shape design that undergoes shape deformation upon external stimulation. The inspiration for such designs can be traced back to strain engineering of roll-up multi-layered microtubes, or self-folding stimuli responsive microrobots presented previously in literature.[97,98] However, in their research, the authors used the photothermal activation of various MOFs to trigger motion.[99] The locomotion was sparked by the removal of solvent molecules from the MOFs' pores upon exposure to UV-Vis light within short time frames. The resulting swelling behaviour of MIL-88A (Materials Institut Lavoisiers, iron(III) fumarate) and its reconfiguration between its open and closed forms is presented in Figure 7a. The combination of MIL-88A into a non-responsive, passive polyvinylidene difluoride (PVDF) matrix and selective etching of the MOF in certain areas, resulted in the creation of passive and active domains in MIL-88A@PVDF films (Figure 7b). Due to the gradients of MIL-88A crystals between the passive and active domains, the films were able to fold when exposed to humidity owing to the different swelling ratios of the areas. This way the authors were able to show that the swelling of the MOF, when exposed to a highly humid environment, could be translated to the macroscopic folding of the film.[96] Selective etching of the MOF and versatile engineering of the passive and active areas allowed the researchers to develop 2D and 3D patterns that can undergo shape transformations and ultimately allow a controlled locomotion of the films (Figure 7c). It is important to highlight here

that the controlled locomotion upon UV-Vis light stimulation was only achieved via multiple cycles of expansion and contraction in a controlled environment (Figure 7d).[60]

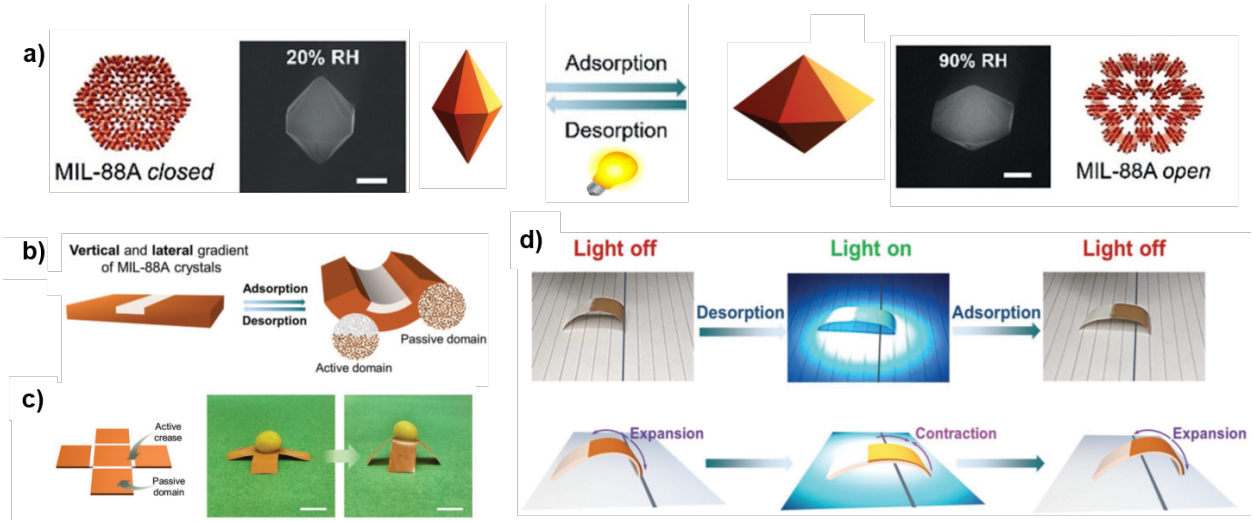

Figure 7. Photothermal response of MIL-88A@PVDF films. a) Schematic of the swelling behaviour of MIL-88A, together with the corresponding environmental FESEM images showing the structural transformation of a single crystal of MIL-88A at relative humidity values of 20% (left) and 90% (right). Desorption can be triggered via irradiation with UV–Vis light. b) Patterning of MIL-88A@PVDF films by chemical etching with HCl allows the development of active and passive domains. c) Schematic and photographs of a patterned MIL-88A@PVDF open-cube structure lifting cargo that is five-times heavier, upon exposure to 90% relative humidity. Scale bars 5 mm. d) Photographs (top) and schematic (bottom) of the walking motion of a patterned MIL-88A@PVDF strip in response to alternating on/off cycles of UV–Vis irradiation. Interlinear spacing: 5 mm. Adapted with permission from ref [60,96] Copyright 2019,2018 John Wiley and Sons.

Even though this work presents a great step towards combining active MOFs with polymers for small-scale robotic applications, constraints arise from the photothermal swelling and de-

swelling mechanism of the MOF. The use of light shows great potential for actuating devices in optically accessible media, but its applicability is limited in opaque media. More specifically, UV-Vis light can only be implemented in surface related applications as it cannot penetrate more than a few millimetres into the human body. Accordingly, the translation of light triggered MOF-based systems into the biomedical domain is particularly challenging.

5. Magnetically driven MOF-based swimmers

Magnetic manipulation is one the most promising approaches for the remote control of small-scale swimmers.[100] Magnetic fields are safe in a wide range of conditions and can penetrate numerous materials, living tissues and organisms, such as the human body.[101] Therefore, magnetic micro- and nanoswimmers have shown great potential in various applications, ranging from targeted delivery of therapies to environmental remediation.[102–104] Additionally, magnetic energy can be transferred in the form of magnetic field gradients, rotating and oscillating magnetic fields, or combinations of these, thus allowing a wealth of manoeuvring strategies.[105] For extended information in magnetic manipulation of magnetic small-scale robots, we refer the readers to some recent contribution in this area.[7] Here, we will briefly comment on the effect of external magnetic fields and magnetic field gradients on magnetic materials.[106] When a magnetic flux density gradient $\nabla\mathbf{B}$ is applied to a magnetic object (i.e.: paramagnetic, diamagnetic, ferro- and ferrimagnetic, superparamagnetic), it experiences a force ($\mathbf{F}$) that is directly proportional to $\nabla\mathbf{B}$ and its net magnetic dipole moment ($\mathbf{m}$):

$$\mathbf{F} = (\mathbf{m} \cdot \nabla)\mathbf{B}$$

Note that $\mathbf{m}$ may be developed when the material is subject to the field, or it may exhibit a remnant magnetic moment that can be further enhanced (only for ferromagnetic materials). When a magnetic object is subject to a homogenous magnetic flux density $\mathbf{B}$, a magnetic torque ($\boldsymbol{\tau}$) will

act on the object, which will cause a change in its orientation so that its **m** is aligned parallel with the direction of the external magnetic field. The amount of **τ** is proportional to **B** and **m** and is expressed as follows:

$$\boldsymbol{\tau} = \mathbf{m} \times \mathbf{B}$$

Magnetic field gradients are usually used to pull magnetic objects with positive magnetic susceptibilities (χ) or push those with negative χ (diamagnetic objects).[107] In contrast, with a suitable object architecture, rotating and oscillating magnetic fields can be applied to achieve different locomotion mechanisms.[108–111]

While magnetic fields represent a versatile approach for micro- and nanorobotic manipulation, research in magnetically driven MOFs has mainly been limited to drag magnetic composite MOF-based particles using magnetic field gradients.[112–115] Strictly speaking, the first magnetically driven MOFBOT was recently reported by Pané, Puigmartí and co-workers.[116] A layer-by-layer fabrication approach was implemented on top of a helical polymeric chassis (Figure 8a), which was subsequently coated with nanometre-thick layers of Ni and Ti. Ni was used for magnetic manipulation, while Ti served as a protective biocompatible coating. Next, the Ti surface was treated with polydopamine, which ultimately enabled the binding of ZIF-8 on the helical chassis of the microswimmer. A fluorescent model drug (Rhodamine-B) was encapsulated *in situ* during the synthesis of the ZIF-8 layer. Using rotating magnetic fields, the MOFBOT was able to move by corkscrew locomotion in biologically relevant fluids and target a single cell using an external magnetic navigation system (Figure 8b). Additionally, because of the fast hydrolysis of ZIF-8 in acidic media, the microrobots displayed pH-dependent drug release capabilities. The authors demonstrated this feature in a specially designed microfluidic platform (Figure 8c-e). The microfluidic system simulated, in terms of pH, extracellular regions corresponding to healthy

tissues (pH = 7) and regions mimicking the extracellular media of tumours (pH = 5). A group of swimmers was magnetically manipulated in this microfluidic system. The swimmers that reached the region with a pH=5 were able to release the cargo, while those that remained at the neutral pH region preserved the drug. This was confirmed from the fluorescence of the model drug.

However, the fate of such microrobots in future *in vivo* applications has still to be addressed. The stiff polymeric core (IP-L 780) and the deposited metal layers of Ni and Pt may have proven this MOFBOT biocompatible *in vitro* within short time frames, but prolonged retention in a living organism may lead to unknown challenges. Biodegradable materials can be implemented to address such issues as they can be degraded and excreted from the body. Biodegradable MOFBOTs for targeted drug delivery have been recently developed by the same group.[117] The researchers implemented organomineralised magnetic Fe@ZIF-8 composite particles, which were produced in a simple one-pot synthesis. The Fe@ZIF-8 crystals were successfully integrated on the surface of soft gelatine-based helical microchassis. In this microrobotic ensemble, Fe@ZIF-8 plays a dual role, acting both as a drug carrier and as an active component for magnetically controlled locomotion. The integrated MOFBOT can be steered under rotating magnetic fields, perform stimuli responsive drug release, and degrade in cell culture over the course of two weeks.

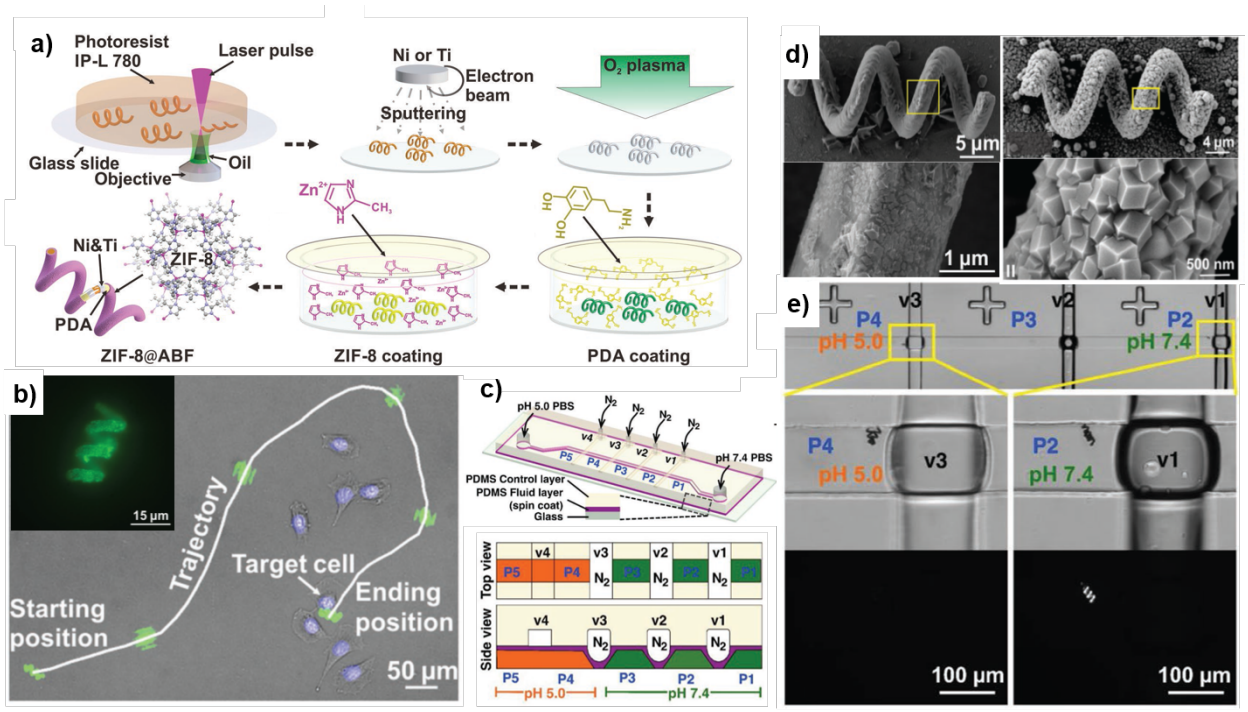

Figure 8. Magnetically driven MOF based swimmers for targeted drug delivery. a) Schematic illustration of MOFBOT fabrication, showing the individual steps followed for the multilayer material design. b) Microscopy images overlay showing the movement of a MOFBOT along a complex trajectory, targeting a single cell. The microrobot is loaded with a fluorescent model drug as shown in the inlet. c) Schematic illustration of the microfluidic setup used to demonstrate pH responsive delivery of cargo. Top and side view of the microfluidic device, indicating the integrated valves. d) Comparative SEM images of ZIF-8@ABFs showing pH responsive degradation of ZIF-8 coating before (right) and after (left) incubation in acidic pH for 12 h. e) Optical and fluorescence microscopy images showing controlled locomotion of MOFBOTs in the microfluidic chip, and selective drug delivery in the acidic pH region. Adapted with permission from ref [116] Copyright 2019 John Wiley and Sons.

6. Biocompatibility of MOF-based swimmers

The potential biocompatibility and toxicity of MOF-based swimmers is considered an important feature in both biomedical and environmental applications. In Table 1, we summarise the main components of these swimmers, the responsive materials involved, their type of propulsion, as well as their potential toxicity in the context of relevant applications. We discriminate between the biocompatibility features of the materials comprising the swimmers, and the environmental requirements for their motion. With this distinction, we highlight the differences between swimmers that can operate in physiological conditions, in contrast to those that for their motion require the presence of certain chemicals in their surroundings.

The Marangoni propelled MOF-based swimmers presented in Section 2 seem to require very specific conditions to operate, such as a gas-liquid interface or a pH gradient. Their locomotion is significantly limited by the amount of fuel they are able to carry, and their function strongly depends on the environment to fuel correlation/interactions. So far, they have not been investigated in the context of a specific application, and therefore their practical implementation is still vague. Similarly, the function of the MOF-based light actuators can be affected by the humidity in the surrounding environment. They have been tested in air, with direct UV-Vis illumination, but so far, we could not find any proof of principle application. Furthermore, certain wavelengths such as UV can potentially harm cells and tissues.[118]

Catalytically propelled MOF motors could exhibit, in principle, optimal biocompatibility features if their constituents are rationally chosen. For example, MOF-based swimmers built of ZIF-8 and Pt could be a good option taking into consideration the biocompatibility characteristics of the underlying materials. However, for their motion, these swimmers require H_2O_2 in concentrations up to 25 % v/v, which are fuel concentrations definitely not applicable in

physiological media, as H_2O_2 is toxic to living organisms.[119] Alternatively, catalytically propelled machines that utilise enzymes for propulsion can be an alternative. It has been shown that motors functionalised with catalase can swim in ultralow concentrations of H_2O_2 that were not toxic to cells in vitro.[83]

Magnetically propelled MOF based swimmer's biocompatibility and biodegradability strongly depends on their underlying components. Examples of both short-term biocompatible and long-term biodegradable MOFBOTs have been presented in the literature. Magnetic MOFBOTs can swim in liquid and physiologically relevant medium, achieving targeting and local degradation in drug delivery applications. Their implementation in biomedical applications has so far shown promising results in the field of targeted drug delivery.[116,117]

Table 1. List of MOF based swimmers and actuators, summarising their underlying components, stimuli response, type of propulsion and where applicable proof-of-principle (PoP) application.

MOF	Responsive Component	Stimulus	Type of Propulsion	PoP Applications	Materials' Biocompatibility / Toxicity [a]	Environmental Requirements [b]	Ref
ZIF-8	Pt	H_2O_2 fuel	Catalytic	–	++	+	78
	Ag	H_2O_2 fuel	Catalytic	Water remediation	++	+	79
	MnO_2 Fe_3O_4 NPs	H_2O_2 fuel Magnetic field	Catalytic Magnetic steering	Water remediation	++	+	87
	Pt Fe_3O_4 NPs	H_2O_2 fuel Magnetic field	Catalytic Magnetic steering	Water remediation	++	+	88
	Ni	Magnetic field	Magnetic steering	Drug delivery *in vitro*	+	+++	116
	Fe-based NPs	Magnetic field	Catalytic Magnetic steering	Drug delivery *in vitro*	+++	+++	117
	Catalase	H_2O_2 fuel	Catalytic	Cancer treatment (ST and PDT) *in vitro*	+++	++	80
ZIF-67	Co - MOF sites	H_2O_2 fuel	Catalytic	–	+	+	77

	Co - MOF sites Fe_3O_4 NPs	H_2O_2 fuel Magnetic field	Catalytic Magnetic steering	Drug delivery *in vitro*	+	+	86
ZIF-L	Catalase β-lactoglobulin	H_2O_2 fuel pH	Catalytic On/off chemical control	Drug delivery *in vitro*	++	+++	82
	Catalase PDPA polymer	H_2O_2 fuel pH	Catalytic Vertical motion control	Drug delivery *in vitro*	++	+++	83
UiO-67	Co, Mn EDTA, IDA	H_2O_2 fuel Chelation	Catalytic Chemical speed control	–	+	+	63
UiO-66	Pt	H_2O_2 fuel	Catalytic	–	++	+	78
MIL-88A	MOF Pores	UV-Light	Swelling / Contraction of MOF pores	–	++	++	60
Cu_2L_2ted	MOF framework	EDTA – MOF degradation – Fuel release pH	Surface tension gradient Directional motion	–	+	++	70
PCN-222	MOF framework	Fuel release Shape Fuel type	Surface tension gradient Directional motion Speed control	–	+	++	71

[a] The materials' biocompatibility for every system is assessed with (+++) for biocompatible and biodegradable components, (++) for biocompatible but non-degradable components, (+) for biocompatible in short-term but potentially long-term toxicity due to components degradation (i.e.: Co, Ni, etc.). [b] The environmental requirements are characterised with (+++) for physiological conditions, (++) for very specific conditions (pH gradient, air-liquid interface, etc.) and (+) for toxic H_2O_2 concentrations.

7. MOFs bearing "supramolecular gadgets"

In the field of small-scale swimmers, motion has been a central aspect of investigation, especially during the last two decades. Efforts at furnishing these devices with other functional tools in order to create highly integrated devices are currently under development. As such, the integration of molecular gadgets in small-scale swimmers is among the next natural steps in the field of small-scale swimmers, and, even more, in the field of MOF-based swimmers. In addition to the prototypical features of MOFs (e.g. their high porosity or swelling properties, as demonstrated in previous examples), MOFs are highly versatile materials, whose structures allow for incorporating molecular engines that not only can act as relevant components for controlling the motion of the swimmers (i.e.: paddles, brakes), but can also supplement additional functionalities such as control over loading/release of cargoes, regulation on the MOF's network dimensions. The incorporation of molecular gadgets with MOFs not only enables stimuli-responsive control of MOFs at the molecular level, but can also impact the device's functionality at the macroscale. The methods for achieving such functionality include modification of the MOF linkers, for example, with the inclusion of molecular machines within the MOF structure, or surface functionalisation of MOFs with stimuli-responsive supramolecular systems. Previous reviews have focused on MOF modifications that enable switching functionality,[55] or purely on supramolecular rotors, motors and machines.[56] Here, we highlight only examples where function is externally controlled and where these MOFs bearing "supramolecular gadgets" can be further considered in future biomedical applications.

7.1. Modification of MOF linkers

A clear example of the incorporation of a supramolecular gadget into a MOF structure was reported by Feringa, Wezenberg, Browne and co-workers in 2019. In this work, the authors describe the

development of a so-called "moto-MOF" that contains linker units that can be rotated through application of an external light stimulus.[59] This was achieved using BrYO-MOF crystals, which are constructed using zinc paddlewheel nodes bridged with tetracarboxylic acid linkers and connected by 4,4′-bipyridine-derived pillars (Figure 9a,c). BrYO-MOF was chosen in this study to ensure enough free space was available in the pores to allow the motor unit to rotate (Figure 9d). The rotation was initiated through the application of UV light, which lead to a change in the conformation of the linker molecule to a metastable state, which then switched back when the light source was removed. Thermal isomerisation was also possible, converting the metastable state to a stable one, which could subsequently be switched to a different metastable state upon application of light. A final treatment with heat of this metastable state returned the linker molecule to its initial stable state, demonstrating the possibility of a controlled and complete cycle through different structural states of the linker molecule by applying external stimuli (Figure 9f).

Feringa *et al*. then extended the potential applications for such a device by creating a similar system in which visible light could be used to drive the motion instead of UV-light.[120] This was achieved through "linker-to-linker" energy transfer, where a palladium-porphyrin linker acted as the light-responsive element, which could absorb the visible light and then transfer this energy through emission to the motor-linker, to induce rotation (Figure 9b,c,e).

While these works do not demonstrate a specific application for such MOFs yet, they could be integrated into systems to control the diffusion of gases, or as pumps in microfluidic devices, as just two potential applications, and classical molecular dynamics simulations have been reported to investigate the feasibility.[121] However, one limitation of these MOF structures is that they are reportedly not stable when the solvent is removed, which potentially limits their applications to those in which the MOF device is constantly solvated. Therefore, these 'moto-MOFs' have the

potential to mature in the future towards controlled artificial living matter or devices for biomedical applications.

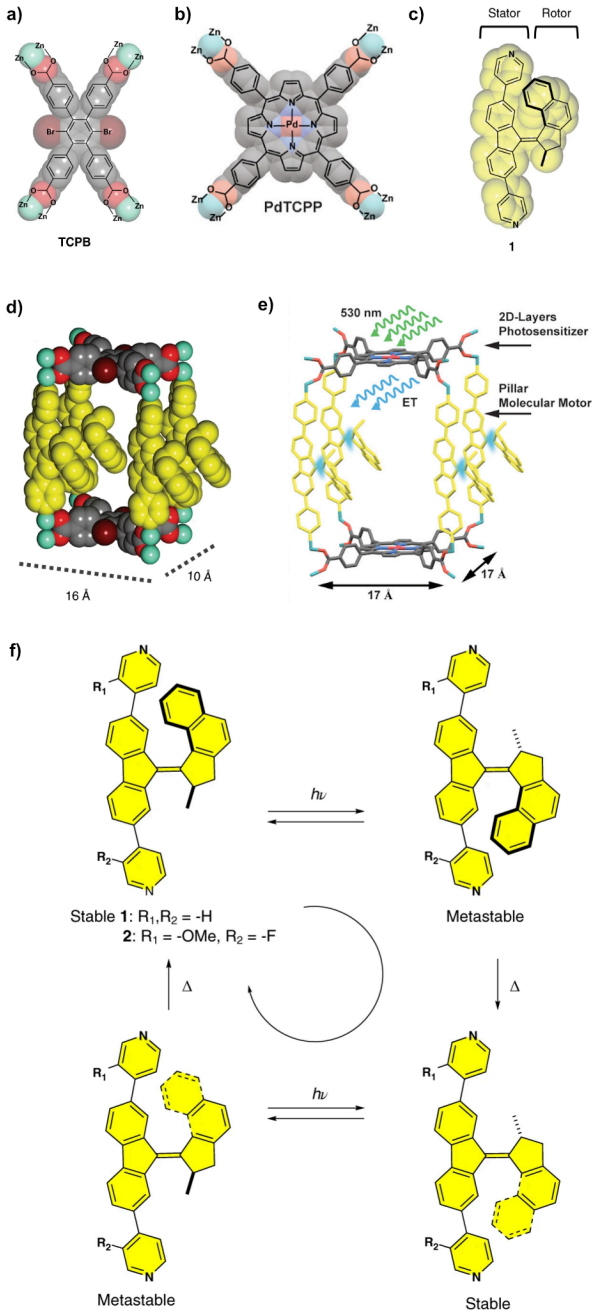

Figure 9. UV- and visible light-driven "moto-MOFs". a) Tetracarboxylic acid (**TCPB**) linker structure for UV-driven moto-MOF. b) Porphyrin-based photosensitiser (**PdTCPP**) linker structure for visible light driven moto-MOF. c) Molecular motor bipyridine linker unit used in both moto-MOF structures. d)

Structure of one unit of UV light driven MOF. e) Schematic illustration of irradiation of MOF with visible light at 530 nm that is absorbed by the porphyrin-based linker, which then transfers the energy to the motor linker to induce rotation. f) Structures of motors **1** and **2**, and light-powered 360° unidirectional rotary cycle of the motor. a,c,d,f) Adapted with permission from Springer Nature ref[59] Copyright 2019. b,e) Adapted from ref[120] Copyright 2020 American Chemical Society.

7.2. Surface functionalisation of MOFs

An alternative approach to introducing external stimuli-responsiveness to MOFs is to functionalise the surface of the MOF crystals. This approach was demonstrated in the work of Nagata *et al*., where UiO-66 crystals were functionalised with poly(N-isopropylacrylamide) (PNIPAM) to act as a thermo-responsive element in the MOF structure.[64] At low temperatures below the cloud point of PNIPAM (i.e. below 32 ºC), the polymer adopts a coil conformation, and the pores of the MOF are accessible for guest release. At temperatures above this point, the polymer conformation changes to a collapsed globule, and guest release is much slower from the pores as the polymer blocks the access (Figure 10a). This was demonstrated using three guests resorufin, caffeine and procainamide. While at 25 ºC, over 70 % of each guest was released in 1 day and almost 100 % release was achieved after 7 days, at 40 ºC at most 20 % of the guests were released during the same time period (Figure 10b). The ability to control the release in a stepwise manner by switching the temperature to open and close the pores was also demonstrated, indicating that the precise release of the guests is achievable with this MOF system where a thermo-responsive "supramolecular gadget" was considered. This functionality demonstrates an effective storage and release system which when integrated with other functionalities could lead to an effective MOF-based micro- and nanoswimmer for transport and delivery of cargo, for example, in drug delivery applications.

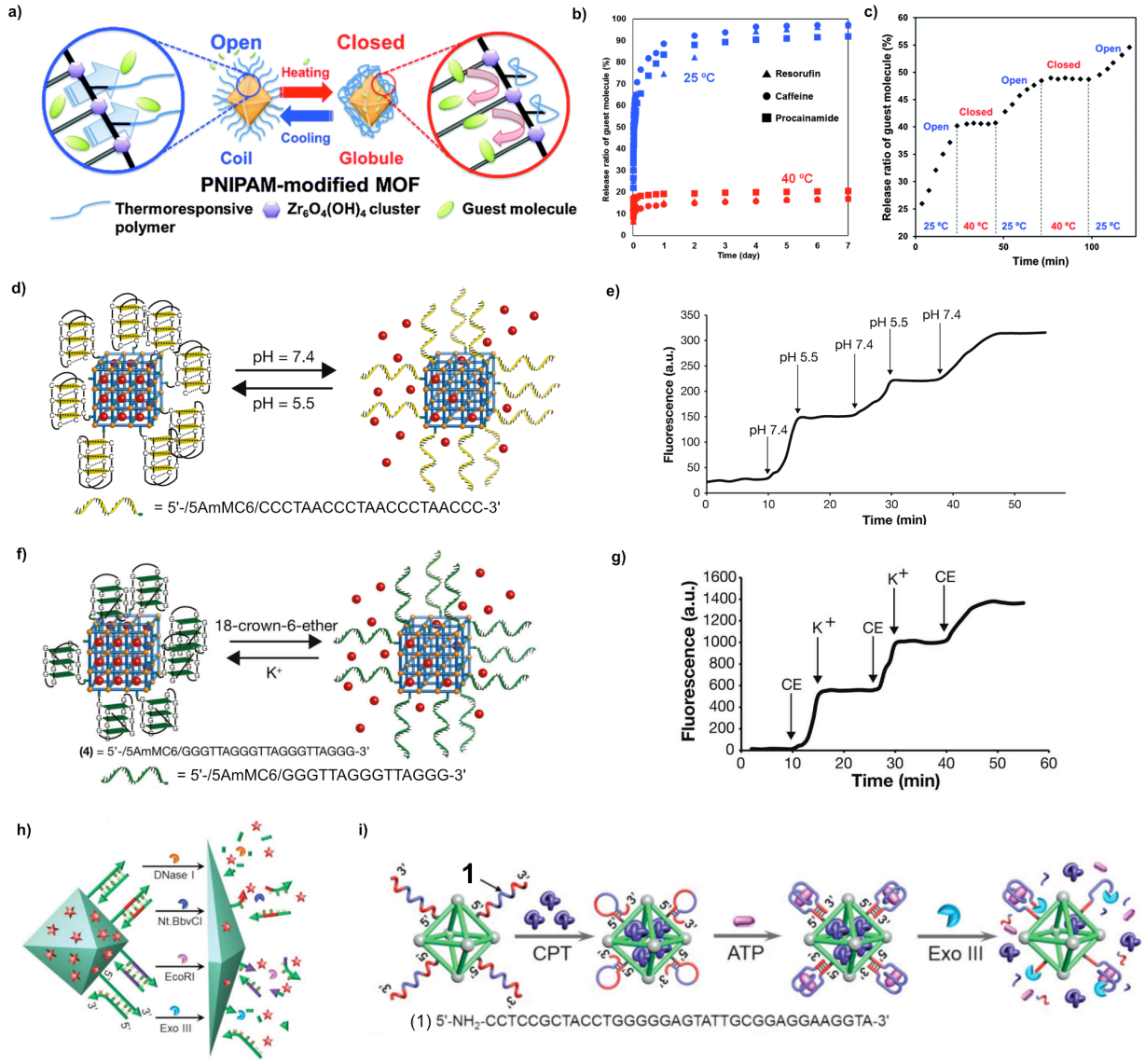

Figure 10. a) Schematic illustration of PNIPAM-modified UiO-66 MOF. At low temperatures the MOF is "open" as the polymer is in the coil conformation, allowing host-guest exchange. Upon heating the polymer changes conformation to a collapsed globule, switching the MOF to "closed" and preventing guest entry or exit. b) Percentage of guest released over time at temperature below the cloud point, 25 ºC, and above the cloud point, 40 ºC, for the three guest molecules studied. c) Stepwise release over time of resorufin guest from the MOF in water by varying the temperature. d) Schematic illustration of DNA functionalised MOF and pH-responsive switchable binding and release of guest molecules. e) Graph showing the increase in

fluorescence observed as the guest is released, with controlled on-off switching – On at pH 7.4, Off at pH 5.5. f) Schematic illustration of DNA functionalised MOF and K^+ ion-responsive switchable binding and release of guest molecules. g) Graph showing the increase in fluorescence observed as the guest is released, with controlled on-off switching. On upon addition of 18-crown-6-ether, Off upon addition of K^+. h) Schematic illustration of DNA functionalised MOF and enzyme interactions leading to release of guest molecules. i) Schematic illustration of guest binding of camptothecin (CPT) into the MOF, formation of the hairpin complex to lock the pores followed by reconfiguration of the hairpin complex in the presence of ATP to form the ATP-aptamer complex, which is then cleaved by Exo III to release the drug. a) to c) adapted with permission from ref[64] Copyright 2015 Royal Society of Chemistry. d-g) Adapted with permission from ref[62] Copyright 2016 John Wiley and Sons. h) and i) Adapted with permission from ref[61] Copyright 2018 John Wiley and Sons.

A similar functionalisation approach was adopted by Willner, Garcia and co-workers, who reported the formation of DNA-functionalised MOF structures which were responsive to pH or K^+ ions.[62] This was achieved using nucleic acid sequences that could assemble into and disassemble from i-motif and duplex DNA nanostructures in response to pH, and a sequence that would form a G-quadruplex structure when K^+ ions were added. The MOF used in this investigation was synthesised by connecting zinc-carboxylate clusters with two organic ligands, i.e. amino terephthalic acid and 4,4′,4″-benzene-1,3,5-triyl-tribenzoic acid. The resulting Zn-based MOF was loaded with rhodamine 6G dye to observe the encapsulation and release behaviour of the MOF structure upon application of the external stimulus. For the i-motif-gated MOFs, the dye was loaded at pH 7.4, at which the nucleic acid existed in a random coil conformation, and so the MOF pores were accessible for uptake of the dye, i.e. a continuous exchange of dye molecules into and out of the structure was possible. However, upon application of an acidic solution, at pH 5.5, the

MOF pores were locked by the i-motif structure of the nucleic acid which effectively prevented release of the dye. Subsequent treatment of the MOF at pH 7.4 caused dissociation of the i-motif, and the dye was released (Figure 10d). Further treatment of the MOF at pH 5.5 could reform the i-motif structure, switching off further release until the MOF was again treated at pH 7.4, with further on-off switching behaviour possible until all of the guest was released (Figure 10e). This demonstrates an effective system for switchable pH-responsive binding and release behaviour of guest molecules, something that could be extended to potential biomedical applications.

A similar mechanism was employed to lock the dye inside the MOF by adding a triplex DNA structure to the solution at pH 7.4, which then formed a duplex structure with a different nucleic acid attached to the MOF to block the pores, after which an acidic solution was added to trigger guest release, thus providing a pH-responsive MOF that was activated at acidic pH rather than neutral, as in the previous example. However, this release was not switchable, and once the MOF had been unlocked, it could not then be relocked to re-trap the dye.

Finally, the functionalisation of the MOF structure presented in this study with a third nucleic acid sequence allowed for the formation of a G-quadruplex structure upon the addition of K^+ ions, which locked the dye in the pores. The addition of 18-crown-6-ether allowed the nucleic acid strand to return to a random coil structure, as the crown-ether chelates the K^+ ions, enabling this system to be reversibly switched upon the addition of K^+ or crown-ether. (Figure 10f,g) Further investigations have also reported similar functionalisation with nucleic acids on ZIF-8, where the addition of K^+ ions releases dye molecules from the MOF structure after being locked in using a DNA capping unit.[122]

In further investigations, Willner and co-workers reported UiO-68-based MOFs functionalised with nucleic acid strands that were responsive to a variety of enzymes as a way of

controlling guest release.[61] UiO-68 crystals were synthesised by the reaction of $ZrCl_4$ with amino-terphenyl dicarboxylic acid. Interestingly, this MOF system bearing nucleic acid strands presented a new way to avoid introducing metal ions,[123] or having to rely on pH to achieve a control release of its cargo. Instead, these MOF crystals provided structures for which only a specific enzyme would unlock the structure, thus providing a method of selectivity to the guest release. The enzymes studied in this work were DNase I, a nicking enzyme (Nt.BbvCI), an endonuclease (EcoRI) and an exonuclease III (Exo III), where each unlocked the MOF pores to release a loaded drug molecule (i.e. camptothecin (CPT)) from specifically functionalised MOFs (Figure 10h). The researchers also expanded the complexity of the stimulus response, such that the nucleic acid capping units first required activation through exposure to a cellular biomarker, before biocatalytic interaction with the strand would release the contained guest. This was demonstrated using ATP and Exo III, where the hairpin structure of the nucleic acid was reconfigured in the presence of ATP to one in which the Exo III enzyme could then digest, triggering guest release (Figure 10i). This coupled stimuli-response provides a potential application in drug delivery systems to cancer cells. The higher proportion of ATP found in cancer cells would enable a selective release to this type of cells, potentially avoiding unwanted side effects. Indeed experiments comparing the cell viability of normal breast epithelial cells (MCF-10A) and breast cancer cells (MDA-MB-231) revealed a decrease of ~55 % for the cancer cells when exposed to the drug-loaded MOFs, compared to only 15 % decrease in viability of the normal cells after 5 days.

Rather than using covalent or coordination interactions to functionalise the surface of MOFs to add stimuli-responsiveness, Gao *et al*. utilised electrostatic interactions between a polycationic polymer and UiO-66 crystals to produce a potential functional device for photodynamic therapy and cell imaging.[124] This system uses a biscyclometalated iridium(III)

complex as a photosensitiser which reacts with molecular oxygen to produce reactive oxygen species (ROS) and cytotoxic singlet oxygen, in order to kill cancer cells upon irradiation of the photosensitiser with light. However, since the iridium complex is toxic even in the absence of light radiation, the researchers used the MOF structure to encapsulate it to improve biocompatibility, and then introduced the stimuli-responsive polymers as a mechanism to control its release (Figure 11a). Specifically, the tri-copolymer used in this work was made from three components: poly[(2-acryloyl)ethyl(p-boronic acid pinacol ester benzyl)-diethylammonium bromide] (BP); poly[2-(5,5-dimethyl-1,3-dioxan-2-yloxy)ethyl acrylate] (PDM); and cyclodextrin-functionalised poly(glycerol methacrylate) (PG) (Figure 11b-d).[125] The BP and PDM components provided the stimuli-responsiveness, with the former changing from positively to negatively charged in the presence of ROS, and the latter changing from hydrophobic at physiological pH ~7 to hydrophilic when at endosomal pH ~ 5. This means that upon irradiating the device once it has been internalised into the cell, ROS are produced allowing it to begin escaping from the endosome and triggering the charge change in the polymer, which changed the electrostatic interaction from attraction to repulsion, accelerating the release of the Ir(III) complex inside the cell. The increased hydrophilicity of the polymer also allowed it to become more soluble in the aqueous environment of the cell, further enhancing the release of the complex into the cellular environment.

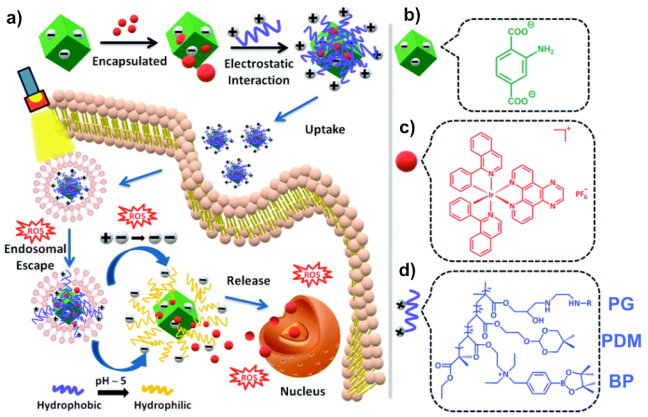

Figure 11. Polycationic polymer functionalised UiO-66 MOF. a) Schematic illustration of the encapsulation of the iridium complex into the MOF structure and association of the polymer to the surface via electrostatic interaction, followed by subsequent uptake into a cell and encapsulation within an endosome. Irradiation of the device leads to reactive oxygen species (ROS) generation, triggering release from the endosome and the polymer becoming negatively charged, leading to increased repulsion between the polymer and the MOF, and hence dissociation. The acidic pH of the cellular environment also changes the polymer from hydrophobic to hydrophilic, further allowing Ir(III) guest complex release. b) Schematic representation of UiO-66 MOF and the linker structural formula. c) Schematic representation of iridium complex and the structural formula. d) Schematic representation of the polymer and structural formula. Reprinted with permission from ref[124] Copyright 2019 Royal Society of Chemistry.

While in this last section we have shown the emergence of a new family of stimuli-responsive MOF-based matter, locomotion, steerability and/or speed control properties are still absent in these systems, and consequently, they cannot yet qualify as MOFBOTs. However, we believe that this marriage of highly porous MOF structures with supramolecular machinery will provide new opportunities in the journey from lab-based case studies to real life biomedical scenarios.

8. Conclusions/Outlook

In the last two decades, MOFs have emerged as an intense area of research where different topologies, adjustable pore sizes and shapes, as well as multiple functions have been described as a result of the nearly limitless number of ligands that can be used for their synthesis. This high degree of tuneability in MOFs has proved essential for achieving substantial fundamental insights that can now be extended to other research domains, such as micro- and nanorobotics. In particular, it has recently been shown that MOF-based devices can also be used to mimic human sensation, a function that represents a major challenge in the field of intelligent robotics.[126] Therefore, it is clear that MOFs are rapidly moving into new terrains in which function is no longer only determined by its building blocks or by their synergistic action, but by an orchestrated response to specific environments or stimuli, just like living matter. This overall concept has been highlighted throughout this manuscript where the modest number of contributions presented so far leads us to believe that we have only gently scratched the surface of MOF-based artificial living matter. The potential use of MOFs in biomedical applications has been demonstrated, where motion of the MOF-based systems has provided a tangible benefit over traditional MOFs, whether by increasing the diffusivity of the MOF-based system, allowing a more effective uptake into cells, or where the controlled directionality has allowed for more specific targeting at a cellular level. In environmental applications, the main use reported to date is the removal of pollutant substances from water, either by degrading them *in situ* or by absorbing them into the MOF network for subsequent removal with the small-scale motor. Even so, many other applications of non-MOF-based micro/nanomotors have been demonstrated in both of these areas, with devices being used to remove a wider range of organic pollutants, nerve agents or heavy metals, or to sense biomarkers to allow for more targeted drug delivery, through performing on-the-fly chemistry.[5,127,128] The

benefits of MOFs with their porous structure, tuneable pore size and shape, and variety of ligand and metal ion combinations means that combined with the propulsion mechanisms already possible, an even broader range of applications should be achievable in areas such as local diagnosis, (bio-)sensing, catalysis, extraction or phytoremediation. Therefore, we believe that there is plenty of room for improvement and innovation in this domain in the years to come.

Additionally, even though the number of methods used to synthesise MOF crystals is increasing each year, there are still some features that cannot be fully controlled during MOF synthesis, such as the concentration, location and nature of defects present in the MOF framework. For example, although molecular machinery other than that previously presented in Section 7 has been incorporated into MOF crystals (e.g. rotaxanes and catenanes),[129,130] their position and number are still random inside the MOF matrix, a result that leads to unpredictable and uncontrollable functions. In contrast, a technology that allowed for controlled defect engineering of a MOF crystal and the precise incorporation of one or multiple molecular shuttles (and/or motors) at specific locations in the MOF matrix, would enabled the assembly of a new generation of interlocked material, where predictable and consistent functions could be accomplished, as in a combustion engine. In this context, multiple molecular machines incorporated in a rational manner and inside a single MOF crystal could work together to achieve a targeted function. Further research in this direction is, therefore, required to create the grounds for a rational design of advanced and unprecedented MOF-based "living matter". Undoubtedly, progress in this realm of functional matter will enable a great number of potential applications in multiple fields, including MOF-based micro- and nanoscale swimmers for biomedical applications.

Acknowledgements

The authors would like to acknowledge funding from the European Research Council Starting Grant microCrysFact (ERC-2015-STG No. 677020), Consolidator Grant HINBOTs (Grant Agreement No. 771565), ETH Grant MOFBOTs (No.ETH-33 17-1) and the Swiss National Science Foundation (Project No.200021_181988). B.J.N. acknowledges the European Research Council Advanced Grant 743217–Soft Micro Robotics (SOMBOT).

Abbreviations

ATP	Adenosine 5'-triphosphate
BA	Benzoic acid
BP	Poly[(2-acryloyl)ethyl(p-boronic acid pinacol ester benzyl)-diethylammonium bromide]
CAT	Catalase
CPT	Camptothecin
DBF	Dibutylformamide
DEF	Diethylformamide
DMF	Dimethylformamide
DOX	Doxorubin hydrochloride
DPA	Diphenylalanine
EDTA	Ethylenediaminetetraacetic acid
GOx	Glucose oxidase
IDA	Iminodiacetic acid
MIL-88A	Materials Institut Lavoisiers – 88A
MOF(s)	Metal-organic framework(s)
PDM	poly[2-(5,5-dimethyl-1,3-dioxan-2-yloxy)ethyl acrylate]
PDPA	Poly(2-diisopropylamino)ethyl methacrylate
PDT	Photodynamic therapy
PG	Poly(glycerol methacrylate)
PNIPAM	Poly(N-isopropylacrylamide)
QD(s)	Quantum dot(s)

ROS	Reactive oxygen species
ST	Starvation therapy
UiO-66	Universitet i Oslo MOF -66
UiO-67	Universitet i Oslo MOF -67
ZIF-8	Zeolitic imidazolate framework – 8
ZIF-67	Zeolitic imidazolate framework - 67

References

(1) Fernández-Medina, M.; Ramos-Docampo, M. A.; Hovorka, O.; Salgueiriño, V.; Städler, B. Recent Advances in Nano- and Micromotors. *Adv. Funct. Mater.* **2020**, *30*, 1908283.

(2) Nelson, B. J.; Kaliakatsos, I. K.; Abbott, J. J. Microrobots for Minimally Invasive Medicine. *Annu. Rev. Biomed. Eng.* **2010**, *12*, 55–85.

(3) Yuan, K.; Jiang, Z.; Jurado-Sánchez, B.; Escarpa, A. Nano/Micromotors for Diagnosis and Therapy of Cancer and Infectious Diseases. *Chem. – Eur. J.* **2020**, *26*, 2309–2326.

(4) Pacheco, M.; López, M. Á.; Jurado-Sánchez, B.; Escarpa, A. Self-Propelled Micromachines for Analytical Sensing: A Critical Review. *Anal. Bioanal. Chem.* **2019**, *411*, 6561–6573.

(5) Karshalev, E.; Esteban-Fernández de Ávila, B.; Wang, J. Micromotors for "Chemistry-on-the-Fly." *J. Am. Chem. Soc.* **2018**, *140*, 3810–3820.

(6) Jurado-Sánchez, B.; Wang, J. Micromotors for Environmental Applications: A Review. *Environ. Sci. Nano* **2018**, *5*, 1530–1544.

(7) Chen, X.-Z.; Hoop, M.; Mushtaq, F.; Siringil, E.; Hu, C.; Nelson, B. J.; Pané, S. Recent Developments in Magnetically Driven Micro- and Nanorobots. *Appl. Mater. Today* **2017**, *9*, 37–48.

(8) Loget, G.; Kuhn, A. Electric Field-Induced Chemical Locomotion of Conducting Objects. *Nat. Commun.* **2011**, *2*, 535.

(9) Rao, K. J.; Li, F.; Meng, L.; Zheng, H.; Cai, F.; Wang, W. A Force to Be Reckoned With: A Review of Synthetic Microswimmers Powered by Ultrasound. *Small* **2015**, *11*, 2836–2846.

(10) Xu, T.; Xu, L.-P.; Zhang, X. Ultrasound Propulsion of Micro-/Nanomotors. *Appl. Mater. Today* **2017**, *9*, 493–503.

(11) Palagi, S.; Singh, D. P.; Fischer, P. Light-Controlled Micromotors and Soft Microrobots. *Adv. Opt. Mater.* **2019**, *7*, 1900370.

(12) Šípová-Jungová, H.; Andrén, D.; Jones, S.; Käll, M. Nanoscale Inorganic Motors Driven by Light: Principles, Realizations, and Opportunities. *Chem. Rev.* **2020**, *120*, 269–287.

(13) Yuan, K.; de la Asunción-Nadal, V.; Jurado-Sánchez, B.; Escarpa, A. 2D Nanomaterials Wrapped Janus Micromotors with Built-in Multiengines for Bubble, Magnetic, and Light Driven Propulsion. *Chem. Mater.* **2020**, *32*, 1983–1992.

(14) Chen, X.-Z.; Jang, B.; Ahmed, D.; Hu, C.; Marco, C. D.; Hoop, M.; Mushtaq, F.; Nelson, B. J.; Pané, S. Small-Scale Machines Driven by External Power Sources. *Adv. Mater.* **2018**, *30*, 1705061.
(15) Wang, J.; Dong, R.; Wu, H.; Cai, Y.; Ren, B. A Review on Artificial Micro/Nanomotors for Cancer-Targeted Delivery, Diagnosis, and Therapy. *Nano-Micro Lett.* **2019**, *12*, 11.
(16) Yim, S.; Gultepe, E.; Gracias, D. H.; Sitti, M. Biopsy Using a Magnetic Capsule Endoscope Carrying, Releasing, and Retrieving Untethered Microgrippers. *IEEE Trans. Biomed. Eng.* **2014**, *61*, 513–521.
(17) Ergeneman, O.; Chatzipirpiridis, G.; Pokki, J.; Marin-Suárez, M.; Sotiriou, G. A.; Medina-Rodriguez, S.; Sanchez, J. F. F.; Fernandez-Gutiérrez, A.; Pane, S.; Nelson, B. J. In Vitro Oxygen Sensing Using Intraocular Microrobots. *IEEE Trans. Biomed. Eng.* **2012**, *59*, 3104–3109.
(18) Mushtaq, F.; Guerrero, M.; Sakar, M. S.; Hoop, M.; Lindo, A. M.; Sort, J.; Chen, X.; Nelson, B. J.; Pellicer, E.; Pané, S. Magnetically Driven Bi2O3/BiOCl-Based Hybrid Microrobots for Photocatalytic Water Remediation. *J. Mater. Chem. A* **2015**, *3*, 23670–23676.
(19) Vilela, D.; Parmar, J.; Zeng, Y.; Zhao, Y.; Sánchez, S. Graphene-Based Microbots for Toxic Heavy Metal Removal and Recovery from Water. *Nano Lett.* **2016**, *16*, 2860–2866.
(20) Ozin, G. A.; Manners, I.; Fournier-Bidoz, S.; Arsenault, A. Dream Nanomachines. *Adv. Mater.* **2005**, *17*, 3011–3018.
(21) Ebbens, S. J.; Howse, J. R. In Pursuit of Propulsion at the Nanoscale. *Soft Matter* **2010**, *6*, 726–738.
(22) Wang, J.; Manesh, K. M. Motion Control at the Nanoscale. *Small* **2010**, *6*, 338–345.
(23) Mei, Y.; Solovev, A. A.; Sanchez, S.; Schmidt, O. G. Rolled-up Nanotech on Polymers: From Basic Perception to Self-Propelled Catalytic Microengines. *Chem. Soc. Rev.* **2011**, *40*, 2109–2119.
(24) Avron, J. E.; Gat, O.; Kenneth, O. Optimal Swimming at Low Reynolds Numbers. *Phys. Rev. Lett.* **2004**, *93*, 186001.
(25) Sitti, M. Miniature Soft Robots — Road to the Clinic. *Nat. Rev. Mater.* **2018**, *3*, 74–75.
(26) Palagi, S.; Fischer, P. Bioinspired Microrobots. *Nat. Rev. Mater.* **2018**, *3*, 113–124.
(27) Erkoc, P.; Yasa, I. C.; Ceylan, H.; Yasa, O.; Alapan, Y.; Sitti, M. Mobile Microrobots for Active Therapeutic Delivery. *Adv. Ther.* **2019**, *2*, 1800064.
(28) Wang, S.; Liu, X.; Wang, Y.; Xu, D.; Liang, C.; Guo, J.; Ma, X. Biocompatibility of Artificial Micro/Nanomotors for Use in Biomedicine. *Nanoscale* **2019**, *11*, 14099–14112.
(29) Li, J.; Esteban-Fernández de Ávila, B.; Gao, W.; Zhang, L.; Wang, J. Micro/Nanorobots for Biomedicine: Delivery, Surgery, Sensing, and Detoxification. *Sci. Robot.* **2017**, *2*, eaam6431.
(30) Yan, Y.; Jing, W.; Mehrmohammadi, M. Photoacoustic Imaging to Track Magnetic-Manipulated Micro-Robots in Deep Tissue. *Sensors* **2020**, *20*, 2816.
(31) Li, D.; Liu, C.; Yang, Y.; Wang, L.; Shen, Y. Micro-Rocket Robot with All-Optic Actuating and Tracking in Blood. *Light Sci. Appl.* **2020**, *9*, 84.
(32) Wang, X.; Qin, X.-H.; Hu, C.; Terzopoulou, A.; Chen, X.-Z.; Huang, T.-Y.; Maniura-Weber, K.; Pané, S.; Nelson, B. J. 3D Printed Enzymatically Biodegradable Soft Helical Microswimmers. *Adv. Funct. Mater.* **2018**, *28*, 1804107.

(33) Tyagi, M.; Spinks, G. M.; Jager, E. W. H. 3D Printing Microactuators for Soft Microrobots. *Soft Robot*. **2020**. https://doi.org/10.1089/soro.2019.0129.
(34) Yang, G.-Z.; Fischer, P.; Nelson, B. New Materials for Next-Generation Robots. *Sci. Robot*. **2017**, *2*, eaap9294.
(35) Tung, H.-W.; Maffioli, M.; Frutiger, D. R.; Sivaraman, K. M.; Pané, S.; Nelson, B. J. Polymer-Based Wireless Resonant Magnetic Microrobots. *IEEE Trans. Robot*. **2014**, *30*, 26–32.
(36) Peng, F.; Tu, Y.; Men, Y.; Hest, J. C. M. van; Wilson, D. A. Supramolecular Adaptive Nanomotors with Magnetotaxis Behavior. *Adv. Mater*. **2017**, *29*, 1604996.
(37) Liu, M.; Liu, L.; Gao, W.; Su, M.; Ge, Y.; Shi, L.; Zhang, H.; Dong, B.; Li, C. Y. A Micromotor Based on Polymer Single Crystals and Nanoparticles: Toward Functional Versatility. *Nanoscale* **2014**, *6*, 8601–8605.
(38) Banerjee, H.; Suhail, M.; Ren, H. Hydrogel Actuators and Sensors for Biomedical Soft Robots: Brief Overview with Impending Challenges. *Biomimetics* **2018**, *3*, 15.
(39) Jeon, S.-J.; Hauser, A. W.; Hayward, R. C. Shape-Morphing Materials from Stimuli-Responsive Hydrogel Hybrids. *Acc. Chem. Res*. **2017**, *50*, 161–169.
(40) Sato, Y.; Hiratsuka, Y.; Kawamata, I.; Murata, S.; Nomura, S. M. Micrometer-Sized Molecular Robot Changes Its Shape in Response to Signal Molecules. *Sci. Robot*. **2017**, *2*, eaal3735.
(41) Snezhko, A.; Aranson, I. S. Magnetic Manipulation of Self-Assembled Colloidal Asters. *Nat. Mater*. **2011**, *10*, 698–703.
(42) Medina-Sánchez, M.; Magdanz, V.; Guix, M.; Fomin, V. M.; Schmidt, O. G. Swimming Microrobots: Soft, Reconfigurable, and Smart. *Adv. Funct. Mater*. **2018**, *28*, 1707228.
(43) Field, R. D.; Anandakumaran, P. N.; Sia, S. K. Soft Medical Microrobots: Design Components and System Integration. *Appl. Phys. Rev*. **2019**, *6*, 041305.
(44) Ou, J.; Liu, K.; Jiang, J.; Wilson, D. A.; Liu, L.; Wang, F.; Wang, S.; Tu, Y.; Peng, F. Micro-/Nanomotors toward Biomedical Applications: The Recent Progress in Biocompatibility. *Small* **2020**, *16*, 1906184.
(45) Wu, Z.; Lin, X.; Zou, X.; Sun, J.; He, Q. Biodegradable Protein-Based Rockets for Drug Transportation and Light-Triggered Release. *ACS Appl. Mater. Interfaces* **2015**, *7*, 250–255.
(46) Wu, M.-X.; Yang, Y.-W. Metal–Organic Framework (MOF)-Based Drug/Cargo Delivery and Cancer Therapy. *Adv. Mater*. **2017**, *29*, 1606134.
(47) Lu, W.; Wei, Z.; Gu, Z.-Y.; Liu, T.-F.; Park, J.; Park, J.; Tian, J.; Zhang, M.; Zhang, Q.; Iii, T. G.; et al. Tuning the Structure and Function of Metal–Organic Frameworks via Linker Design. *Chem. Soc. Rev*. **2014**, *43*, 5561–5593.
(48) Peh, S. B.; Karmakar, A.; Zhao, D. Multiscale Design of Flexible Metal–Organic Frameworks. *Trends Chem*. **2020**, *2*, 199–213.
(49) Wang, Y.; Yan, J.; Wen, N.; Xiong, H.; Cai, S.; He, Q.; Hu, Y.; Peng, D.; Liu, Z.; Liu, Y. Metal-Organic Frameworks for Stimuli-Responsive Drug Delivery. *Biomaterials* **2020**, *230*, 119619.
(50) Chowdhuri, A. R.; Bhattacharya, D.; Kumar Sahu, S. Magnetic Nanoscale Metal Organic Frameworks for Potential Targeted Anticancer Drug Delivery, Imaging and as an MRI Contrast Agent. *Dalton Trans*. **2016**, *45*, 2963–2973.

(51) Böll, K.; Zimpel, A.; Dietrich, O.; Wuttke, S.; Peller, M. Clinically Approved MRI Contrast Agents as Imaging Labels for a Porous Iron-Based MOF Nanocarrier: A Systematic Investigation in a Clinical MRI Setting. *Adv. Ther.* **2020**, *3*, 1900126.
(52) Banerjee, S.; Lollar, C. T.; Xiao, Z.; Fang, Y.; Zhou, H.-C. Biomedical Integration of Metal–Organic Frameworks. *Trends Chem.* **2020**, *2*, 467–479.
(53) McKinlay, A. C.; Morris, R. E.; Horcajada, P.; Férey, G.; Gref, R.; Couvreur, P.; Serre, C. BioMOFs: Metal–Organic Frameworks for Biological and Medical Applications. *Angew. Chem. Int. Ed.* **2010**, *49*, 6260–6266.
(54) Khezri, B.; Pumera, M. Metal–Organic Frameworks Based Nano/Micro/Millimeter-Sized Self-Propelled Autonomous Machines. *Adv. Mater.* **2019**, *31*, 1806530.
(55) Bigdeli, F.; Lollar, C. T.; Morsali, A.; Zhou, H.-C. Switching in Metal–Organic Frameworks. *Angew. Chem. Int. Ed.* **2020**, *59*, 4652–4669.
(56) Martinez-Bulit, P.; Stirk, A. J.; Loeb, S. J. Rotors, Motors, and Machines Inside Metal–Organic Frameworks. *Trends Chem.* **2019**, *1*, 588–600.
(57) Hassan, Z.; Matt, Y.; Begum, S.; Tsotsalas, M.; Bräse, S. Assembly of Molecular Building Blocks into Integrated Complex Functional Molecular Systems: Structuring Matter Made to Order. *Adv. Funct. Mater.* **2020**, *30*, 1907625.
(58) Ikezoe, Y.; Washino, G.; Uemura, T.; Kitagawa, S.; Matsui, H. Autonomous Motors of a Metal-Organic Framework Powered by Reorganization of Self-Assembled Peptides at Interfaces. *Nat. Mater.* **2012**, *11*, 1081–1085.
(59) Danowski, W.; van Leeuwen, T.; Abdolahzadeh, S.; Roke, D.; Browne, W. R.; Wezenberg, S. J.; Feringa, B. L. Unidirectional Rotary Motion in a Metal–Organic Framework. *Nat. Nanotechnol.* **2019**, *14*, 488–494.
(60) Troyano, J.; Carné-Sánchez, A.; Maspoch, D. Programmable Self-Assembling 3D Architectures Generated by Patterning of Swellable MOF-Based Composite Films. *Adv. Mater.* **2019**, *31*, 1808235.
(61) Chen, W.-H.; Luo, G.-F.; Sohn, Y. S.; Nechushtai, R.; Willner, I. Enzyme-Driven Release of Loads from Nucleic Acid–Capped Metal–Organic Framework Nanoparticles. *Adv. Funct. Mater.* **2019**, *29*, 1805341.
(62) Kahn, J. S.; Freage, L.; Enkin, N.; Garcia, M. A. A.; Willner, I. Stimuli-Responsive DNA-Functionalized Metal–Organic Frameworks (MOFs). *Adv. Mater.* **2017**, *29*, 1602782.
(63) Li, J.; Yu, X.; Xu, M.; Liu, W.; Sandraz, E.; Lan, H.; Wang, J.; Cohen, S. M. Metal–Organic Frameworks as Micromotors with Tunable Engines and Brakes. *J. Am. Chem. Soc.* **2017**, *139*, 611–614.
(64) Nagata, S.; Kokado, K.; Sada, K. Metal–Organic Framework Tethering PNIPAM for ON–OFF Controlled Release in Solution. *Chem. Commun.* **2015**, *51*, 8614–8617.
(65) Purcell, E. M. Life at Low Reynolds Number. *Am. J. Phys.* **1977**, *45*, 3–11.
(66) Weibull, C. Movement of Bacterial Flagella. *Nature* **1951**, *167*, 511–512.
(67) Wilkinson, P. C. Chemotaxis. In *Encyclopedia of Immunology (Second Edition)*; Delves, P. J.; Elsevier: Oxford, 1998; pp 533–537.
(68) Tadmor, R. Marangoni Flow Revisited. *J. Colloid Interface Sci.* **2009**, *332*, 451–454.
(69) Peyer, K. E.; Zhang, L.; Nelson, B. J. Bio-Inspired Magnetic Swimming Microrobots for Biomedical Applications. *Nanoscale* **2013**, *5*, 1259–1272.
(70) Ikezoe, Y.; Fang, J.; Wasik, T. L.; Shi, M.; Uemura, T.; Kitagawa, S.; Matsui, H. Peptide–Metal Organic Framework Swimmers That Direct the Motion toward Chemical Targets. *Nano Lett.* **2015**, *15*, 4019–4023.

(71) Park, J. H.; Lach, S.; Polev, K.; Granick, S.; Grzybowski, B. A. Metal–Organic Framework "Swimmers" with Energy-Efficient Autonomous Motility. *ACS Nano* **2017**, *11*, 10914–10923.
(72) Sánchez, S.; Soler, L.; Katuri, J. Chemically Powered Micro- and Nanomotors. *Angew. Chem. Int. Ed Engl.* **2015**, *54*, 1414–1444.
(73) Mirkovic, T.; Zacharia, N. S.; Scholes, G. D.; Ozin, G. A. Nanolocomotion—Catalytic Nanomotors and Nanorotors. *Small* **2010**, *6*, 159–167.
(74) Li, L.; Wang, J.; Li, T.; Song, W.; Zhang, G. Hydrodynamics and Propulsion Mechanism of Self-Propelled Catalytic Micromotors: Model and Experiment. *Soft Matter* **2014**, *10*, 7511–7518.
(75) Paxton, W. F.; Kistler, K. C.; Olmeda, C. C.; Sen, A.; St. Angelo, S. K.; Cao, Y.; Mallouk, T. E.; Lammert, P. E.; Crespi, V. H. Catalytic Nanomotors: Autonomous Movement of Striped Nanorods. *J. Am. Chem. Soc.* **2004**, *126*, 13424–13431.
(76) Safdar, M.; Khan, S. U.; Jänis, J. Progress toward Catalytic Micro- and Nanomotors for Biomedical and Environmental Applications. *Adv. Mater.* **2018**, *30*, 1703660.
(77) Tan, T. T. Y.; Cham, J. T. M.; Reithofer, M. R.; Hor, T. S. A.; Chin, J. M. Motorized Janus Metal Organic Framework Crystals. *Chem. Commun. Camb. Engl.* **2014**, *50*, 15175–15178.
(78) Ayala, A.; Carbonell, C.; Imaz, I.; Maspoch, D. Introducing Asymmetric Functionality into MOFs via the Generation of Metallic Janus MOF Particles. *Chem. Commun.* **2016**, *52*, 5096–5099.
(79) Wang, R.; Guo, W.; Li, X.; Liu, Z.; Liu, H.; Ding, S. Highly Efficient MOF-Based Self-Propelled Micromotors for Water Purification. *RSC Adv.* **2017**, *7*, 42462–42467.
(80) You, Y.; Xu, D.; Pan, X.; Ma, X. Self-Propelled Enzymatic Nanomotors for Enhancing Synergetic Photodynamic and Starvation Therapy by Self-Accelerated Cascade Reactions. *Appl. Mater. Today* **2019**, *16*, 508–517.
(81) Aebi, H. Catalase. In *Methods of Enzymatic Analysis (Second Edition)*; Bergmeyer, H. U.; Academic Press, 1974; Vol. 2, pp 673–684.
(82) Gao, S.; Hou, J.; Zeng, J.; Richardson, J. J.; Gu, Z.; Gao, X.; Li, D.; Gao, M.; Wang, D.-W.; Chen, P.; et al. Superassembled Biocatalytic Porous Framework Micromotors with Reversible and Sensitive pH-Speed Regulation at Ultralow Physiological H_2O_2 Concentration. *Adv. Funct. Mater.* **2019**, *29*, 1808900.
(83) Guo, Z.; Wang, T.; Rawal, A.; Hou, J.; Cao, Z.; Zhang, H.; Xu, J.; Gu, Z.; Chen, V.; Liang, K. Biocatalytic Self-Propelled Submarine-like Metal-Organic Framework Microparticles with pH-Triggered Buoyancy Control for Directional Vertical Motion. *Mater. Today* **2019**, *28*, 10–16.
(84) Willott, J. D.; Humphreys, B. A.; Murdoch, T. J.; Edmondson, S.; Webber, G. B.; Wanless, E. J. Hydrophobic Effects within the Dynamic pH-Response of Polybasic Tertiary Amine Methacrylate Brushes. *Phys. Chem. Chem. Phys.* **2015**, *17*, 3880–3890.
(85) Solovev, A. A.; Sanchez, S.; Pumera, M.; Mei, Y. F.; Schmidt, O. G. Magnetic Control of Tubular Catalytic Microbots for the Transport, Assembly, and Delivery of Micro-Objects. *Adv. Funct. Mater.* **2010**, *20*, 2430–2435.
(86) Wang, L.; Zhu, H.; Shi, Y.; Ge, Y.; Feng, X.; Liu, R.; Li, Y.; Ma, Y.; Wang, L. Novel Catalytic Micromotor of Porous Zeolitic Imidazolate Framework-67 for Precise Drug Delivery. *Nanoscale* **2018**, *10*, 11384–11391.

(87) Liu, J.; Li, J.; Wang, G.; Yang, W.; Yang, J.; Liu, Y. Bioinspired Zeolitic Imidazolate Framework (ZIF-8) Magnetic Micromotors for Highly Efficient Removal of Organic Pollutants from Water. *J. Colloid Interface Sci.* **2019**, *555*, 234–244.
(88) Ying, Y.; Pourrahimi, A. M.; Sofer, Z.; Matějková, S.; Pumera, M. Radioactive Uranium Preconcentration via Self-Propelled Autonomous Microrobots Based on Metal–Organic Frameworks. *ACS Nano* **2019**, *13*, 11477–11487.
(89) Mathesh, M.; Sun, J.; Wilson, D. A. Enzyme Catalysis Powered Micro/Nanomotors for Biomedical Applications. *J. Mater. Chem. B* **2020**, *8*, 7319–7334.
(90) Patiño, T.; Arqué, X.; Mestre, R.; Palacios, L.; Sánchez, S. Fundamental Aspects of Enzyme-Powered Micro- and Nanoswimmers. *Acc. Chem. Res.* **2018**, *51*, 2662–2671.
(91) Pantarotto, D.; Browne, W. R.; Feringa, B. L. Autonomous Propulsion of Carbon Nanotubes Powered by a Multienzyme Ensemble. *Chem. Commun.* **2008**, 1533–1535.
(92) Karshalev, E.; Esteban-Fernández de Ávila, B.; Beltrán-Gastélum, M.; Angsantikul, P.; Tang, S.; Mundaca-Uribe, R.; Zhang, F.; Zhao, J.; Zhang, L.; Wang, J. Micromotor Pills as a Dynamic Oral Delivery Platform. *ACS Nano* **2018**, *12*, 8397–8405.
(93) Darwin Palima, J. G. *Light Robotics - Structure-Mediated Nanobiophotonics*, 1st ed.; Nanophotonics; Elsevier, 2017.
(94) Pustovalov, V. K.; Smetannikov, A. S.; Zharov, V. P. Photothermal and Accompanied Phenomena of Selective Nanophotothermolysis with Gold Nanoparticles and Laser Pulses. *Laser Phys. Lett.* **2008**, *5*, 775–792.
(95) Behl, M.; Lendlein, A. Actively Moving Polymers. *Soft Matter* **2006**, *3*, 58–67.
(96) Troyano, J.; Carné-Sánchez, A.; Pérez-Carvajal, J.; León-Reina, L.; Imaz, I.; Cabeza, A.; Maspoch, D. A Self-Folding Polymer Film Based on Swelling Metal–Organic Frameworks. *Angew. Chem. Int. Ed.* **2018**, *57*, 15420–15424.
(97) Magdanz, V.; Stoychev, G.; Ionov, L.; Sanchez, S.; Schmidt, O. G. Stimuli-Responsive Microjets with Reconfigurable Shape. *Angew. Chem.* **2014**, *126*, 2711–2715.
(98) Fusco, S.; Sakar, M. S.; Kennedy, S.; Peters, C.; Bottani, R.; Starsich, F.; Mao, A.; Sotiriou, G. A.; Pané, S.; Pratsinis, S. E.; et al. An Integrated Microrobotic Platform for On-Demand, Targeted Therapeutic Interventions. *Adv. Mater.* **2014**, *26*, 952–957.
(99) Espín, J.; Garzón-Tovar, L.; Carné-Sánchez, A.; Imaz, I.; Maspoch, D. Photothermal Activation of Metal–Organic Frameworks Using a UV–Vis Light Source. *ACS Appl. Mater. Interfaces* **2018**, *10*, 9555–9562.
(100) Tottori, S.; Zhang, L.; Qiu, F.; Krawczyk, K. K.; Franco-Obregón, A.; Nelson, B. J. Magnetic Helical Micromachines: Fabrication, Controlled Swimming, and Cargo Transport. *Adv. Mater.* **2012**, *24*, 811–816.
(101) Bottomley, P. A.; Andrew, E. R. RF Magnetic Field Penetration, Phase Shift and Power Dissipation in Biological Tissue: Implications for NMR Imaging. *Phys. Med. Biol.* **1978**, *23*, 630–643.
(102) Servant, A.; Qiu, F.; Mazza, M.; Kostarelos, K.; Nelson, B. J. Controlled In Vivo Swimming of a Swarm of Bacteria-Like Microrobotic Flagella. *Adv. Mater.* **2015**, *27*, 2981–2988.
(103) Mushtaq, F.; Chen, X.; Hoop, M.; Torlakcik, H.; Pellicer, E.; Sort, J.; Gattinoni, C.; Nelson, B. J.; Pané, S. Piezoelectrically Enhanced Photocatalysis with BiFeO3 Nanostructures for Efficient Water Remediation. *iScience* **2018**, *4*, 236–246.

(104) Hoop, M.; Ribeiro, A. S.; Rösch, D.; Weinand, P.; Mendes, N.; Mushtaq, F.; Chen, X.-Z.; Shen, Y.; Pujante, C. F.; Puigmartí-Luis, J.; et al. Mobile Magnetic Nanocatalysts for Bioorthogonal Targeted Cancer Therapy. *Adv. Funct. Mater.* **2018**, *28*, 1705920.
(105) Huang, H.-W.; Sakar, M. S.; Petruska, A. J.; Pané, S.; Nelson, B. J. Soft Micromachines with Programmable Motility and Morphology. *Nat. Commun.* **2016**, *7*, 12263.
(106) Abbott, J. J.; Ergeneman, O.; Kummer, M. P.; Hirt, A. M.; Nelson, B. J. Modeling Magnetic Torque and Force for Controlled Manipulation of Soft-Magnetic Bodies. *IEEE Trans. Robot.* **2007**, *23*, 1247–1252.
(107) Yesin, K. B.; Vollmers, K.; Nelson, B. J. Modeling and Control of Untethered Biomicrorobots in a Fluidic Environment Using Electromagnetic Fields: *Int. J. Robot. Res.* **2006**, *25*, 527–536.
(108) Abbott, J. J.; Peyer, K. E.; Lagomarsino, M. C.; Zhang, L.; Dong, L.; Kaliakatsos, I. K.; Nelson, B. J. How Should Microrobots Swim?: *Int. J. Robot. Res.* **2009**, *28*, 1434–1447.
(109) Yim, S.; Sitti, M. Design and Rolling Locomotion of a Magnetically Actuated Soft Capsule Endoscope. *IEEE Trans. Robot.* **2012**, *28*, 183–194.
(110) Khalil, I. S. M.; Dijkslag, H. C.; Abelmann, L.; Misra, S. MagnetoSperm: A Microrobot That Navigates Using Weak Magnetic Fields. *Appl. Phys. Lett.* **2014**, *104*, 223701.
(111) Zhang, L.; Abbott, J. J.; Dong, L.; Kratochvil, B. E.; Bell, D.; Nelson, B. J. Artificial Bacterial Flagella: Fabrication and Magnetic Control. *Appl. Phys. Lett.* **2009**, *94*, 064107.
(112) Elsaidi, S. K.; Sinnwell, M. A.; Banerjee, D.; Devaraj, A.; Kukkadapu, R. K.; Droubay, T. C.; Nie, Z.; Kovarik, L.; Vijayakumar, M.; Manandhar, S.; et al. Reduced Magnetism in Core–Shell Magnetite@MOF Composites. *Nano Lett.* **2017**, *17*, 6968–6973.
(113) Falcaro, P.; Lapierre, F.; Marmiroli, B.; Styles, M.; Zhu, Y.; Takahashi, M.; Hill, A. J.; Doherty, C. M. Positioning an Individual Metal–Organic Framework Particle Using a Magnetic Field. *J. Mater. Chem. C* **2012**, *1*, 42–45.
(114) Lu, G.; Li, S.; Guo, Z.; Farha, O. K.; Hauser, B. G.; Qi, X.; Wang, Y.; Wang, X.; Han, S.; Liu, X.; et al. Imparting Functionality to a Metal–Organic Framework Material by Controlled Nanoparticle Encapsulation. *Nat. Chem.* **2012**, *4*, 310–316.
(115) Falcaro, P.; Normandin, F.; Takahashi, M.; Scopece, P.; Amenitsch, H.; Costacurta, S.; Doherty, C. M.; Laird, J. S.; Lay, M. D. H.; Lisi, F.; et al. Dynamic Control of MOF-5 Crystal Positioning Using a Magnetic Field. *Adv. Mater.* **2011**, *23*, 3901–3906.
(116) Wang, X.; Chen, X.-Z.; Alcântara, C. C. J.; Sevim, S.; Hoop, M.; Terzopoulou, A.; Marco, C. de; Hu, C.; Mello, A. J. de; Falcaro, P.; et al. MOFBOTS: Metal–Organic-Framework-Based Biomedical Microrobots. *Adv. Mater.* **2019**, *31*, 1901592.
(117) Terzopoulou, A.; Wang, X.; Chen, X.-Z.; Palacios-Corella, M.; Pujante, C.; Herrero-Martín, J.; Qin, X.-H.; Sort, J.; deMello, A. J.; Nelson, B. J.; et al. Biodegradable Metal–Organic Framework-Based Microrobots (MOFBOTs). *Adv. Healthc. Mater.* 2001031. https://doi.org/10.1002/adhm.202001031.
(118) Pattison, D. I.; Davies, M. J. Actions of Ultraviolet Light on Cellular Structures. In *Cancer: Cell Structures, Carcinogens and Genomic Instability*; Experientia Supplementum; Birkhäuser: Basel, 2006; Vol. 96, pp 131–157.
(119) Gülden, M.; Jess, A.; Kammann, J.; Maser, E.; Seibert, H. Cytotoxic Potency of H2O2 in Cell Cultures: Impact of Cell Concentration and Exposure Time. *Free Radic. Biol. Med.* **2010**, *49*, 1298–1305.
(120) Danowski, W.; Castiglioni, F.; Sardjan, A. S.; Krause, S.; Pfeifer, L.; Roke, D.; Comotti, A.; Browne, W. R.; Feringa, B. L. Visible-Light-Driven Rotation of Molecular Motors in

a Dual-Function Metal–Organic Framework Enabled by Energy Transfer. *J. Am. Chem. Soc.* **2020**, *142*, 9048–9056.

(121) Evans, J. D.; Krause, S.; Feringa, B. L. Cooperative and Synchronized Rotation in Motorized Porous Frameworks: Impact on Local and Global Transport Properties of Confined Fluids. *Faraday Discuss.* **2020**. https://doi.org/10.1039/D0FD00016G.

(122) Cao, X.; Xia, J.; Meng, X.; Xu, J.; Liu, Q.; Wang, Z. Stimuli-Responsive DNA-Gated Nanoscale Porous Carbon Derived from ZIF-8. *Adv. Funct. Mater.* **2019**, *29*, 1902237.

(123) Chen, W.-H.; Yu, X.; Cecconello, A.; Sohn, Y. S.; Nechushtai, R.; Willner, I. Stimuli-Responsive Nucleic Acid-Functionalized Metal–Organic Framework Nanoparticles Using pH- and Metal-Ion-Dependent DNAzymes as Locks. *Chem. Sci.* **2017**, *8*, 5769–5780.

(124) Zhang, Y.; Fu, H.; Chen, S.; Liu, B.; Sun, W.; Gao, H. Construction of an Iridium(III)-Complex-Loaded MOF Nanoplatform Mediated with a Dual-Responsive Polycationic Polymer for Photodynamic Therapy and Cell Imaging. *Chem. Commun.* **2020**, *56*, 762–765.

(125) Zhu, H.; An, J.; Pang, C.; Chen, S.; Li, W.; Liu, J.; Chen, Q.; Gao, H. A Multifunctional Polymeric Gene Delivery System for Circumventing Biological Barriers. *J. Mater. Chem. B* **2019**, *7*, 384–392.

(126) He, K.; Liu, Y.; Wang, M.; Chen, G.; Jiang, Y.; Yu, J.; Wan, C.; Qi, D.; Xiao, M.; Leow, W. R.; et al. An Artificial Somatic Reflex Arc. *Adv. Mater.* **2020**, *32*, 1905399.

(127) Uygun, D. A.; Jurado-Sánchez, B.; Uygun, M.; Wang, J. Self-Propelled Chelation Platforms for Efficient Removal of Toxic Metals. *Environ. Sci. Nano* **2016**, *3*, 559–566.

(128) Singh, V. V.; Martin, A.; Kaufmann, K.; D. S. de Oliveira, S.; Wang, J. Zirconia/Graphene Oxide Hybrid Micromotors for Selective Capture of Nerve Agents. *Chem. Mater.* **2015**, *27*, 8162–8169.

(129) Gholami, G.; Wilson, B. H.; Zhu, K.; O'Keefe, C. A.; Schurko, R.; Loeb, S. J. Exploring the Dynamics of Zr-Based Metal-Organic Frameworks Containing Mechanically Interlocked Molecular Shuttles. *Faraday Discuss.* **2020**. https://doi.org/10.1039/D0FD00004C.

(130) Zhu, K.; O'Keefe, C. A.; Vukotic, V. N.; Schurko, R. W.; Loeb, S. J. A Molecular Shuttle That Operates inside a Metal–Organic Framework. *Nat. Chem.* **2015**, *7*, 514–519.

Author Biographies

Anastasia Terzopoulou is currently a doctoral candidate at the Multi-Scale Robotics Lab (MSRL), ETH Zürich. She graduated her BSc in Physics in 2016 from Aristotle University of Thessaloniki, with research interest in magnetic nanomaterials, MagnaCharta group. In 2015, she worked as an Erasmus intern at the group for Structure and Magnetism on the Nanoscale, University Duisburg-Essen. In 2017 she received her MSc in Biomedical Engineering, ETH Zürich, after completing her thesis at the Institute of Robotics and Intelligent Systems. Her current research focuses on metal-organic frameworks as functional materials for magnetic microrobots.

James Nicholas is currently a doctoral candidate at ETH Zürich. He received his BA in Natural Sciences from the University of Cambridge in 2017. He then completed an MSc by research at the University of York in 2019, investigating the host-guest chemistry of coordination cages using EPR spectroscopy with Dr Victor Chechik. His current research is focussed on the development of functional materials, through design and synthesis of porous supramolecular networks and investigation of dissipative non-equilibrium systems.

Xiangzhong Chen is currently senior researcher at the Multi-Scale Robotics Lab (MSRL) of the Institute of Robotics and Intelligent Systems (IRIS) at ETH Zürich. He received his Ph.D. in 2013, majoring in polymer chemistry and physics from Nanjing University. In November 2013, he joined in MSRL as a post-doctoral researcher. His Ph.D. thesis is about the application of ferroelectric polymers in the field of data storage, energy storage, and energy conversion. Now he is working on bridging magnetic and ferroelectric materials (ceramics, polymers, and composites) with robotic microdevices for bio-medical applications such as cell stimulation and drug delivery.

Bradley J. Nelson has been the Professor of Robotics and Intelligent Systems at ETH Zürich since 2002. Before moving to Europe, Prof. Nelson worked as an engineer at Honeywell and Motorola and served as a United States Peace Corps Volunteer in Botswana, Africa. He has also been a professor at the University of Minnesota and the University of Illinois at Chicago. He has over thirty years of experience in the field of robotics. He serves on the advisory boards of a number of academic departments and research institutes across North America, Europe, and Asia and is on the editorial boards of several academic journals

Salvador Pané is currently titular professor at ETH Zürich, leading the group of Materials for Robotics, at the Institute of Robotics and Intelligent Systems (IRIS), ETH Zürich. He received his Ph.D. in chemistry (2008) from the Universitat de Barcelona in the field of the electrodeposition of magnetic materials. He became a post-doctoral researcher at IRIS in August 2008 and senior research scientist in 2012. Prof. Pané is currently working on bridging materials science, chemistry, and electrochemistry with small-scale robotics for various applications.

Josep Puigmartí-Luis is a chemist who completed a master in Chemistry and Food Engineering at "Institut Químico de Serrià (IQS)" (2003) and did a PhD in materials science at Institut de Ciència de Materials de Barcelona (ICMAB). In 2012, and after a postdoctoral position at ETH where he was awarded an ETH fellowship, he was appointed a Ramon Y Cajal (RyC) researcher at ICMAB. After two years as a RyC, he decided to move back to Switzerland where in 2015 was awarded an ERC starting grant to study and control self-assembly processes of metal-organic based crystalline materials. His research interests include the synthesis and controlled design of functional materials in solution, as well as the development of microfluidic technologies to command and understand

the formation and function of unprecedented out-of-equilibrium assemblies (a key aspect to unveil structure-properties correlations of new functional matter). In 2019, Prof. Puigmartí-Luis was appointed as an ICREA Professor, and since 2020, his group is located at the University of Barcelona (UB).

TOC Image

(5cm x 5 cm)